Elsevier Editorial System(tm) for European Journal of Medicinal Chemistry
Manuscript Draft

Manuscript Number: EJMECH-D-13-01920R1

Title: 1,2,3,4-Tetrahydrobenzo[h][1,6]naphthyridines as a new family of potent peripheral-to-midgorge-site inhibitors of acetylcholinesterase: synthesis, pharmacological evaluation and mechanistic studies

Article Type: Full Length Article

Keywords: benzo[h][1,6]naphthyridines; Povarov reaction; dual inhibitors; AChE PAS; AChE midgorge binding

Corresponding Author: Prof. Diego Muñoz-Torrero, Doctor in Pharmacy

Corresponding Author's Institution: University of Barcelona

First Author: Diego Muñoz-Torrero, Doctor in Pharmacy

Order of Authors: Diego Muñoz-Torrero, Doctor in Pharmacy; Ornella Di Pietro, PhD student; Elisabet Viayna, Dr.; Esther Vicente-García, Dr.; Manuela Bartolini, Dr.; Rosario Ramón, Dr.; Jordi Juárez-Jiménez, PhD student; M. Victòria Clos, Dr.; Belén Pérez, Dr.; Vincenza Andrisano, Dr.; F. Javier Luque, Dr.; Rodolfo Lavilla, Dr.

Abstract: A series of 1,2,3,4-tetrahydrobenzo[h][1,6]naphthyridines differently substituted at positions 1, 5, and 9 have been designed from the pyrano[3,2-c]quinoline derivative 1, a weak inhibitor of acetylcholinesterase (AChE) with predicted ability to bind to the AChE peripheral anionic site (PAS), at the entrance of the catalytic gorge. Fourteen novel benzonaphthyridines have been synthesized through synthetic sequences involving as the key step a multicomponent Povarov reaction between an aldehyde, an aniline and an enamine or an enamide as the activated alkene. The novel compounds have been tested against Electrophorus electricus AChE (EeAChE), human recombinant AChE (hAChE), and human serum butyrylcholinesterase (hBChE), and their brain penetration has been assessed using the PAMPA-BBB assay. Also, the mechanism of AChE inhibition of the most potent compounds has been thoroughly studied by kinetic studies, a propidium displacement assay, and molecular modelling. We have found that a seemingly small structural change such as a double O → NH bioisosteric replacement from the hit 1 to 16a results in a dramatic increase of EeAChE and hAChE inhibitory activities (>217- and >154-fold, respectively), and in a notable increase in hBChE inhibitory activity (> 11-fold), as well. An optimized binding at the PAS besides additional interactions with AChE midgorge residues seem to account for the high hAChE inhibitory potency of 16a (IC50 = 65 nM), which emerges as an interesting anti-Alzheimer lead compound with potent dual AChE and BChE inhibitory activities.

1,2,3,4-Tetrahydrobenzo[*h*][1,6]naphthyridines as a new family of potent peripheral-to-midgorge-site inhibitors of acetylcholinesterase: synthesis, pharmacological evaluation and mechanistic studies

Ornella Di Pietro[a], Elisabet Viayna[a], Esther Vicente-García[b], Manuela Bartolini[c], Rosario Ramón[b], Jordi Juárez-Jiménez[d], M. Victòria Clos[e], Belén Pérez[e], Vincenza Andrisano[f], F. Javier Luque[d], Rodolfo Lavilla[b,g,*], Diego Muñoz-Torrero[a,**]

[a] *Laboratori de Química Farmacèutica (Unitat Associada al CSIC), Facultat de Farmàcia, and Institut de Biomedicina (IBUB), Universitat de Barcelona, Av. Joan XXIII, 27-31, E-08028, Barcelona, Spain*

[b] *Barcelona Science Park, Baldiri Reixac 10-12, E-08028, Barcelona, Spain*

[c] *Department of Pharmacy and Biotechnology, Alma Mater Studiorum University of Bologna, Via Belmeloro 6, I-40126, Bologna, Italy*

[d] *Departament de Fisicoquímica, Facultat de Farmàcia, and IBUB, Universitat de Barcelona, Prat de la Riba 171, E-08921, Santa Coloma de Gramenet, Spain*

[e] *Departament de Farmacologia, de Terapèutica i de Toxicologia, Institut de Neurociències, Universitat Autònoma de Barcelona, E-08193, Bellaterra, Barcelona, Spain*

[f] *Department for Life Quality Studies, University of Bologna, Corso d'Augusto 237, I-47921, Rimini, Italy*

[g] *Laboratori de Química Orgànica, Facultat de Farmàcia, Universitat de Barcelona, Av. Joan XXIII, 27-31, E-08028, Barcelona, Spain*

* Corresponding author. Tel.: +34 934037106; fax: +34 934024539.

** Corresponding author. Tel.: +34 934024533; fax: +34 934035941.

E-mail addresses: rlavilla@pcb.ub.es (R. Lavilla), dmunoztorrero@ub.edu (D. Muñoz-Torrero).

ABSTRACT

A series of 1,2,3,4-tetrahydrobenzo[*h*][1,6]naphthyridines differently substituted at positions 1, 5, and 9 have been designed from the pyrano[3,2-*c*]quinoline derivative **1**, a weak inhibitor of acetylcholinesterase (AChE) with predicted ability to bind to the AChE peripheral anionic site (PAS), at the entrance of the catalytic gorge. Fourteen novel benzonaphthyridines have been synthesized through synthetic sequences involving as the key step a multicomponent Povarov reaction between an aldehyde, an aniline and an enamine or an enamide as the activated alkene. The novel compounds have been tested against *Electrophorus electricus* AChE (EeAChE), human recombinant AChE (hAChE), and human serum butyrylcholinesterase (hBChE), and their brain penetration has been assessed using the PAMPA-BBB assay. Also, the mechanism of AChE inhibition of the most potent compounds has been thoroughly studied by kinetic studies, a propidium displacement assay, and molecular modelling. We have found that a seemingly small structural change such as a double O → NH bioisosteric replacement from the hit **1** to **16a** results in a dramatic increase of EeAChE and hAChE inhibitory activities (>217- and >154-fold, respectively), and in a notable increase in hBChE inhibitory activity (> 11-fold), as well. An optimized binding at the PAS besides additional interactions with AChE midgorge residues seem to account for the high hAChE inhibitory potency of **16a** (IC_{50} = 65 nM), which emerges as an interesting anti-Alzheimer lead compound with potent dual AChE and BChE inhibitory activities.

Keywords: Benzo[*h*][1,6]naphthyridines
Povarov reaction
Dual inhibitors
AChE PAS binding
AChE midgorge binding

1. Introduction

Alzheimer's disease (AD) is a progressive and ultimately fatal neurodegenerative disorder that is currently threatening every health system worldwide. The number of people with AD increases rapidly, and in line with this, both prevalence and costs are also increasing [1]. Currently, it is estimated that dementia, of which AD is the most common type, is affecting 36 million people, with a total cost amounting to as much as 1% of global gross domestic product [1]. AD is among the top ten causes of death, but, worryingly, the only one that cannot be prevented, cured or slowed down [2], thereby making it imperative the development of efficacious drugs.

Current therapeutic options, i.e. the acetylcholinesterase (AChE) inhibitors donepezil, galantamine and rivastigmine and the glutamate NMDA receptor antagonist memantine, are regarded as merely symptomatic, and very promising β-amyloid (Aβ)-directed drug candidates designed to confront the underlying mechanisms of AD are inexorably failing in late stage clinical trials due to lack of efficacy or safety. The increasingly accepted notion that Aβ is not *the* cause but *one of the* causes of AD [3] is spurring the development of multi-target drugs that simultaneously hit Aβ formation and aggregation as well as other important targets such as tau hyperphosphorylation and aggregation, oxidative stress and cholinesterases, among others, as a more realistic option to effectively treat AD [4].

In every case, any single-target or multi-target drug candidate purported to modify AD progression would need to be administered in the early presymptomatic or preclinical stage of AD, before neurodegeneration is too widespread. Indeed, preclinical AD has been proposed as the initial stage of AD in the new criteria and guidelines for diagnosing AD [2]. Accurate and reliable biomarkers, indicative of the earliest signs of the disease, are necessary both to identify individuals in the presymptomatic stage of AD, amenable to early interventions with disease-modifying drugs and to monitor their effects. Many research endeavours are being made to select the best diagnostic biomarkers or combinations thereof [5] but much more work is still needed before preclinical AD can be diagnosed [2]. Meanwhile, diagnosis of AD will remain based on symptoms, i.e. on the occurrence of cognitive decline, for whose alleviation AChE inhibitors (AChEIs) are the best therapeutic option [6], thereby warranting the search for novel AChEIs.

Most known AChEIs have been designed to interact with the catalytic site of the enzyme, which is placed at the bottom of a 20 Å deep narrow gorge. The entrance of the gorge contains the so-called peripheral anionic site (PAS) [7], which can be also targeted either separately or simultaneously by potential inhibitors [8]. Recently, we have developed a new family of AChEIs that consisted of a pyrano[3,2-*c*]quinoline moiety connected through linkers of different lengths to a unit of the potent active site AChEI 6-chlorotacrine [9]. Among those hybrids, the most potent human AChE (hAChE) inhibitors bore a 5-(4-chlorophenyl)pyrano[3,2-*c*]quinoline moiety, which is present in their synthetic ester precursor **1** (Fig. 1) and is reminiscent to the phenyl-substituted tricyclic system of the AChE PAS inhibitor propidium (**2**, Fig. 1). Not unexpectedly, molecular dynamics simulations suggested that the 5-(4-chlorophenyl)pyrano[3,2-*c*]quinoline moiety of the hybrids interacts at the PAS of AChE, namely by establishing π–π stacking interactions with residues Trp286 and Tyr72 (hAChE numbering), whereas the 6-chlorotacrine unit interacts with the active site residues Trp86 and Tyr337. Strikingly, despite the predicted ability of the 5-(4-chlorophenyl)pyrano[3,2-*c*]quinoline moiety to interact with the AChE PAS, compound **1** was found to be essentially inactive as inhibitor of hAChE (IC_{50} > 10 μM).

In the light of these results, we inferred that substitution of the oxygen atom at position 1 of the pyrano[3,2-*c*]quinoline system of **1** by a nitrogen atom would result in increased basicity of the quinoline nitrogen atom, which would become protonatable at physiological pH. This would enable the resulting benzo[*h*][1,6]naphthyridine system to establish cation–π interactions additionally to the π–π stacking, thereby potentially increasing its affinity for the PAS of AChE and the AChE inhibitory activity. These interactions would be similar to those established by the phenanthridinium system of propidium, but unlike propidium, the non-permanent character of the positive charge at the quinoline nitrogen atom of the benzo[*h*][1,6]naphthyridine system would not preclude their penetration into the central nervous system (CNS).

Herein, we describe the synthesis, cholinesterase inhibitory activity evaluation and a comprehensive assessment of the binding mode to AChE by kinetic, propidium displacement and molecular modelling studies of a series of 1,2,3,4-tetrahydrobenzo[*h*][1,6]naphthyridines differently substituted at positions 1, 5, and 9. Moreover, the brain penetration of these compounds has been assessed using the parallel artificial membrane permeation assay (PAMPA-BBB).

2. Results and discussion

2.1. Synthesis of the target compounds

To assess the effect on cholinesterase inhibitory activity of substitution at position 1, we initially planned the synthesis of 1,2,3,4-benzo[*h*][1,6]naphthyridines bearing an ethyl ester group at position 9 and a 4-chlorophenyl substituent at position 5, like in the pyrano[3,2-*c*]quinoline analogue **1**, and either a benzyl group (**10a**), hydrogen atom (**12a**) or a 4-methoxybenzyl group (**13a**) on the nitrogen atom at position 1 (Scheme 1). Also, to ascertain the effect of the substituent at position 5, we planned the synthesis of the 1-benzylated ethyl ester analogues bearing a 3-pyridyl (**10b**) or 4-methoxycarbonylphenyl (**10c**) substituent at position 5. Finally, to shed light on the role of the substituent at position 9, we studied the substitution of the ethyl carboxylic ester group of **10a** by an *N*-ethyl carboxamide (**14a**) and an ethylaminomethyl (**17a**) group. Following the evaluation of the AChE inhibitory activity of this first generation of 1,2,3,4-benzo[*h*][1,6]naphthyridine derivatives and the establishment of structure–activity relationships, we additionally envisioned the synthesis of compounds **12b**, **16a**, **18a**, and **18b** (Scheme 1) as second generation optimized analogues (see below).

The synthesis of compounds **10a**–**c** was envisaged out through a three-step sequence involving an initial Povarov multicomponent reaction [10] between the known cyclic enamide **3** [11], as the activated alkene, ethyl 4-aminobenzoate, **5**, and the aromatic aldehydes **4a**–**c**, under $Sc(OTf)_3$ catalysis in acetonitrile (Scheme 1). These reactions afforded in moderate to good yields and 1:1 to 1.7:1 diastereomeric ratio the diastereomeric mixtures of *cis*-fused octahydronaphthyridines **6a**–**c**, which were subjected to DDQ oxidation [12] to yield the lactams **9a**–**c** in 73%, 5%, and 36% yield, respectively, after silica gel column chromatography purification. In an attempt to improve the yield of **9b**, the oxidation of the mixture **6b** with MnO_2 [13] instead of DDQ only afforded unreacted material and open-ring byproducts. Chemoselective reduction of lactams **9a**–**c** with $(EtO)_3SiH$ under $Zn(OAc)_2$ catalysis [14] provided the desired benzonaphthyridines **10a**–**c** in low to moderate (15–52%) yields.

Analogously, the Povarov reaction of aniline **5**, aldehydes **4a**,**b** and the commercially available *N*-Boc-protected cyclic enamine **7**, followed by DDQ or MnO_2 oxidation of the resulting diastereomeric mixtures **8a**,**b** afforded the *N*-Boc-protected derivatives **11a** and **11b** in 57% and 24% overall yields (Scheme 1). Acidic deprotection of **11a** quantitatively yielded the target benzonaphthyridine **12a**, which was also used as starting material for the synthesis of the 1-(4-methoxybenzyl)-substituted

benzonaphthyridine **13a** (40% yield) by deprotonation with NaH and alkylation with 1-chloromethyl-4-methoxybenzene. In turn, acidic deprotection of **11b** afforded the target benzonaphthyridine **12b** in 76% yield.

Derivatization at position 9 was carried out following standard procedures. Thus, ethyl carboxylic esters **10a**, **11a** and **12b** were converted into the corresponding *N*-ethylcarboxamides **14a**, **15a** and **16b**, respectively, in moderate overall yields, by alkaline hydrolysis followed by reaction of the resulting carboxylic acids, isolated as naphthyridine hydrochlorides, with ethyl chloroformate in the presence of Et_3N, and reaction of the mixed anhydrides with ethylamine (Scheme 1). Finally, $LiAlH_4$ reduction of the amides **14a** and **16b** afforded the amines **17a** and **18b** in 44% and 51% yields, respectively, whereas reaction of the *N*-Boc-protected amide **15a** with $LiAlH_4$ proceeded with both *N*-Boc-deprotection and reduction of the amide, directly affording the target *N*-Boc-deprotected benzonaphthyridine **18a** in 35% yield, together with a small amount of the *N*-Boc-deprotected amide **16a** (14% yield).

2.2. Biological activity assays

The inhibitory activity of the novel 1,2,3,4-tetrahydrobenzo[*h*][1,6]naphthyridines against *Electrophorus electricus* AChE (EeAChE) and human recombinant (hAChE) was evaluated by the method of Ellman *et al.* [15]. Another cholinesterase that seems to play an important role in the cognitive decline associated to AD is butyrylcholinesterase (BChE). BChE exerts a compensatory effect in response to the decrease of AChE in CNS as AD progresses, thereby making dual inhibition of AChE and BChE a desirable property for anti-Alzheimer drugs [16]. Thus, the inhibitory activity of these compounds against human serum BChE (hBChE) was determined as well [15].

In general, the novel first-generation benzonaphthyridines were found to be moderately potent inhibitors of EeAChE, with IC_{50} values ranging from the submicromolar to the low micromolar range (Table 1). The best substitution pattern at position 1 clearly involves the presence of an unsubstituted secondary amino group, compound **12a** being 23- and >107-fold more potent EeAChE inhibitor than the *N*-benzylated and *N*-(4-methoxy)benzylated counterparts **10a** and **13a**, respectively. With the sole exception of **12a**, the rest of first generation benzonaphthyridines are *N*-benzylated derivatives, among which two additional structure–activity relationship (SAR) trends leading to a higher EeAChE inhibitory activity could be derived, namely the presence of a 3-pyridyl and an ethylaminomethyl substituent at positions 5 and 9, respectively. Thus, the 5-(3-

pyridyl)-substituted ester **10b** is 3-fold more potent that its 5-(4-chlorophenyl)- and 5-(4-methoxycarbonylphenyl)-substituted analogues **10a** and **10c**, whereas the benzonaphthyridine **17a**, bearing an amine functionality in the side chain at position 9, is about 40-fold more potent than the ester and amide derivatives **10a** and **14a** (Table 1). Not unexpectedly, the benzonaphthyridines **10b**,**c** are more potent EeAChE inhibitors than their less basic lactam precursors **9b**,**c** (>15- and 2-fold, respectively), with the exception of compounds **10a** and **9a**, which were roughly equipotent.

In the light of the SAR derived from the first-generation benzonaphthyridines, starting from **10a** we designed a second generation of analogues bearing simultaneously several or all of the structural features that were found to lead to higher EeAChE inhibitory activity, all of them *N*-debenzylated at position 1 and additionally bearing either a 3-pyridyl group at position 5 (**12b**) or an ethylaminoethyl chain at position 9 (**18a**) or both groups (**18b**). To further explore the role of *N*-debenzylation at position 1, compound **16a**, the debenzylated analogue of the amide **14a**, was also included among the second generation benzonaphthyridines.

With the exception of **18a**, which is 4-fold less potent than its *N*-benzylated analogue **17a**, the second-generation *N*-debenzylated benzonaphthyridines **12b** and **16a** were clearly more potent than their *N*-benzylated counterparts **10b** and **14a** (13- and 119-fold, respectively). However, the two SAR trends seen for the first-generation *N*-benzylated benzonaphthyridines were not apparent in the second-generation *N*-debenzylated analogues, in which the presence of a 4-chlorophenyl group at position 5 and an amide functionality at the side chain in position 9 were the structural features leading to an optimal EeAChE inhibitory activity. These results seem to suggest a different orientation of the *N*-benzylated and *N*-debenzylated compounds within EeAChE. Worthy of note, divergent SARs and binding modes of the PAS-binding moiety of two similar structural classes of inhibitors featuring small changes in their aromatic rings have been recently reported [17].

Overall, amide **16a** turned out to be the most potent benzonaphthyridine of the whole series as EeAChE inhibitor, exhibiting a nanomolar IC_{50} value (46 nM).

When tested on hAChE, significant inter-species differences relative to EeAChE were found in some cases, even though similar general SAR trends were observed. Thus, benzonaphthyridines bearing an amide or an amine functionality in the side chain at position 9 were found to be potent inhibitors, with IC_{50} values in the submicromolar range in all cases except for the 5-(3-pyridyl)-substituted derivative **18b**, whereas most

ester derivatives were weakly active (Table 1). Among the most potent derivatives, the higher hAChE inhibitory activity was associated to the presence of an unsubstituted secondary amino group at position 1 (**16a** and **18a** being 12- and 2-fold more potent than **14a** and **17a**), an amide at position 9 (**14a** and **16a** being 1.2- and 9-fold more potent than the amines **17a** and **18a**) and a 4-chlorophenyl substituent at position 5 (**18a** being 28-fold more potent than **18b**). Again, benzonaphthyridine **16a** turned out to be the most interesting compound of the series, emerging as a very potent inhibitor of hAChE (IC_{50} 65 nM). Noteworthy, **16a** is 500-fold more potent than the specific PAS inhibitor propidium and 6-fold more potent than the active site inhibitor tacrine, the second most potent hAChEI among the approved anti-Alzheimer drugs.

Regarding the inhibition of hBChE, most compounds displayed very weak inhibitory activity (4–28% inhibition at 30 μM). Interestingly, the *N*-debenzylated amide or amine derivatives **16a**, **18a**, and **18b** were found to be more potent inhibitors of hBChE, with IC_{50} values around 1–3 μM (Table 1), they being more potent than propidium but less potent than tacrine.

Inhibition of Aβ aggregation is another valuable property for anti-Alzheimer compounds, which is additionally investigated in many cholinesterase inhibitors [19]. Unfortunately, these benzonaphthyridines turned out to be rather weak inhibitors of Aβ42 self-aggregation, displaying percentages of inhibition up to 16% at 10 μM (data not shown).

Overall, benzonaphthyridine **16a** emerges as a promising anti-Alzheimer agent, by virtue of its dual potent hAChE and hBChE inhibitory activities. Because interactions of ligands at the PAS of AChE are not as tight as those that can be established at the active site, peripheral site AChEIs do not usually display high affinities and potencies [20]. Thus, the potent hAChE inhibitory activity of some of the benzonaphthyridines, particularly **16a**, which were designed as peripheral site AChEIs, was somehow astonishing. To shed light on the binding mode of these compounds within AChE, a set of mechanistic studies was performed, encompassing kinetic experiments (Lineweaver-Burk and Cornish-Bowden plots), propidium displacement assay, and molecular modelling studies (docking and molecular dynamics simulations, and Solvated Interaction Energy calculations).

2.3. Kinetic studies

To investigate the mode of inhibition of the most active AChEI benzonaphthyridine, **16a**, and its *N*-benzylated analogue **14a**, Lineweaver-Burk double reciprocal plots were generated. The interception of the lines in the Lineweaver-Burk plot above the x-axis (Fig. 2) demonstrated that both compounds serve as mixed-type inhibitors of AChE. Mixed-type of inhibition was further confirmed by Cornish-Bowden plots (S/*v versus* [I]) [21].

The inhibition constant (K_i) and the K'_i (dissociation constant for the enzyme–substrate–inhibitor complex) estimated for **14a** were 0.785 μM and 2.34 μM, respectively, and for **16a** were 0.065 μM and 0.073 μM, respectively. These findings show that introduction of a benzyl substituent at position 1 decreases the affinity not only for the enzyme active site (12-fold higher dissociation constant of the EI complex) but likely also for the PAS (32-fold higher K'_i value). Moreover, the similar values of K_i and K'_i found for **16a** suggest that the high inhibitory potency of this compound might arise from the ability to tightly bind both sites, and not only at the PAS.

To get further insights into the mechanism of inhibition and confirm the ability to interact with the AChE PAS, the affinity of the four most interesting derivatives (**14a**, **16a**, **17a**, and **18a**) for the PAS of AChE was investigated by displacement studies with propidium iodide, using the method of Taylor *et al.* [22]. Propidium selectively associates with the PAS of AChE exhibiting an eight-fold enhancement of fluorescence [22a,23]. Back-titration experiments with increasing concentration of all selected compounds but **14a** showed a concentration-dependent decrease in the fluorescence intensity associated with the propidium–AChE complex, suggesting that they can effectively displace propidium from the AChE's PAS (Fig. 3A). Solubility of **14a** in the assay conditions was insufficient to allow a full back-titration experiment. At 1/1 ratio with propidium iodide **14a** was able to reduce fluorescence intensity associated with the AChE–propidium complex by only 5%, confirming a lower affinity for the PAS than the *N*-debenzylated analogue **16a**, as also suggested by the K'_i values. In general, the affinity trend was **16a > 18a > 17a** with concentrations required for decreasing initial fluorescence intensity of AChE–propidium complex ([propidium] = 8 μM) equal to 13, 23, and 33 μM, respectively.

Back-titration experiments for the most active derivative in the series, **16a**, predicted a dissociation constant of 1.76 μM (Fig. 3B). This value is consistent with a quite tight binding to the PAS, only 2.5-fold weaker than that of propidium (K_D on *Ee*AChE = 0.7

μM [23]). Values for the other tested analogues were slightly higher, being 2.18 and 3.20 μM for **18a** and **17a**, respectively. The slightly lower value obtained for the *N*-benzylated derivative, **17a**, further confirms an unfavorable effect of the benzyl substituent at position 1.

2.4. Molecular modelling studies

The binding of compounds **16a** and **18a** to hAChE (Fig. 4) was firstly explored by docking calculations carried out with rDock [24]. It is worth noting that previous studies strongly support the performance of this docking program for predicting the binding mode of a number of AChE inhibitors to the enzyme [9]. Docking was performed using three models of hAChE that differ in the orientation of Trp286, which was arranged to reflect the three major conformations adopted by this residue upon inspection of the available X-ray crystallographic structures (see Experimental part) [25].

The docking results revealed a preferential binding to the AChE model where Trp286 retains the orientation found in the AChE–propidium complex (PDB ID 1N5R [20b]). This finding is not unexpected keeping in mind the size of the heteropolycyclic ring system present in compounds **16a** and **18a** and in propidium. Thus, a distinctive binding mode was clearly identified on the basis of the most populated cluster of docked poses and the docking score, where the 5-(4-chlorobenzyl) substituent of **16a** and **18a** stacks against the indole ring of Trp286 and the CONHEt (**16a**) and CH_2NH_2Et (**18a**) substituents penetrate along the gorge towards the catalytic site.

A 100 ns MD simulation was run to refine the binding mode of compounds **16a** and **18a**. Simulations yielded structurally and energetically stable trajectories, which showed an initial rearrangement of the ligand without significant alterations in the residues that shape the binding site (see Fig. S1 in Supplementary material). The results obtained for compound **16a** point out that the central pyridine ring of the benzonaphthyridine system stacks against Trp286 (average distance of 3.74 Å; Fig. 4A), thus enabling the cation-π interaction between the protonated pyridine nitrogen atom of **16a** and the indole system of Trp286. Furthermore, binding is assisted by the formation of hydrogen bonds between the pyridine nitrogen atom and the hydroxyl group of Tyr72 (average distance of 3.20 Å) and between the amide NH group and the hydroxyl group of Tyr124 (average distance of 3.17 Å). Compared to **16a**, binding of **18a** involves the formation of a water-mediated bridge between the protonated amine of the side chain at position 9 and Asp72 (average distance of 5.9 Å) and a cation-π interaction with the benzene ring

of Tyr341 (average distance of 3.54 Å), besides the cation-π interaction with Trp286. Finally, the NH group at position 1 forms water-mediated hydrogen bonds with the carbonyl groups of Ser293 and Phe338. Clearly, the similar binding mode of compounds **16a** and **18a** (Fig. 4B) must be drastically perturbed by the attachment of the *N*-benzyl group at position 1 due to the steric clash with the neighbouring residues, which likely explains the weaker potency measured for compounds **14a** and **17a**. Overall, MD simulations show that compounds **16a** and **18a** are capable of forming a network of diverse interactions with residues at the PAS and midgorge sites.

To further validate the binding mode of **16a** and **18a**, the binding affinities were determined using the Solvated Interaction Energy (SIE) calculations. The SIE method relies on MM/PBSA calculations of the ligand–receptor complex, but the free energy components are weighted by a scaling factor parametrized to reproduce the experimental binding affinities for a diverse set of protein–ligand complexes [26]. The predicted binding affinities for **16a** and **18a** are –8.5 ± 0.4 and –8.8 ± 0.6 kcal/mol (see Table S1 in Supplementary material), which compare with the experimental value determined from the inhibition constant for **16a** (–9.7 kcal/mol). Thus, within the uncertainty of the SIE method, the predicted binding affinities reflect the similar inhibitory potency of **16a** and **18a**. Since they exhibit a similar binding mode, it can be concluded that the large desolvation penalty of the protonated amine present in the side chain at position 9 counterbalances the enhanced coulombic stabilization found for **18a**, the net effect leading to an inhibitory potency close to the potency of the amide derivative **16a**.

2.5. Blood–brain barrier permeation assay

Brain penetration is an essential property for every anti-Alzheimer drug candidate. The ability of the synthesized benzonaphthyridines to cross the blood–brain barrier (BBB) and therefore to reach the CNS was assessed using the known parallel artificial membrane permeation assay (PAMPA-BBB) as an *in vitro* model of passive transcellular permeation [27]. The *in vitro* permeability (P_e) of the novel 1,2,3,4-benzo[*h*][1,6]naphthyridines through a lipid extract of porcine brain was determined using a mixture of phosphate-buffered saline (PBS)/EtOH (70:30). Assay validation was carried out by comparison of the experimental and reported permeability values of 14 commercial drugs (see Table S2 in Supplementary Material), which provided a good linear correlation: P_e (exp) = 1.4974 P_e (lit) – 0.8434 (R^2 = 0.9428). Using this equation

and the limits established by Di *et al.* for BBB permeation [27], the following ranges of permeability were established: P_e (10^{-6} cm s^{-1}) > 5.1 for compounds with high BBB permeation (CNS+); P_e (10^{-6} cm s^{-1}) < 2.15 for compounds with low BBB permeation (CNS–); and 5.1 > P_e (10^{-6} cm s^{-1}) > 2.15 for compounds with uncertain BBB permeation (CNS+/–). All the tested benzonaphthyridines were predicted to be able to cross the BBB, with the exception of amine **18b**, for which an uncertain brain penetration was predicted. Indeed, amines **18b** and **18a**, whose permeability value was near the minimum threshold for high BBB permeation, seemed to be the most polar benzonaphthyridines of the series, which, as mentioned above might account for the apparently high desolvation penalty detrimental for their AChE inhibitory potencies.

3. Conclusion

We have carried out the optimization of the AChE PAS-binding affinity of the initial hit **1**, ethyl 5-(4-chlorophenyl)-3,4-dihydro-2*H*-pyrano[3,2-*c*]quinoline-9-carboxylate, neutral at physiological pH, by replacement of the oxygen atom at position 1 by a nitrogen atom [of a N–H, *N*-benzyl or *N*-(4-methoxybenzyl) group]. The main aim of this structural change was to increase the basicity, and therefore the protonation ability, of the resulting 1,2,3,4-tetrahydrobenzo[*h*][1,6]naphthyridine derivatives, thereby making it possible the establishment of cation-π interactions besides π-π stacking with the PAS residue Trp286. Moreover, the effect on the AChE inhibitory activity of replacements of the 4-chlorophenyl and ethyl carboxylate groups at positions 5 and 9, present in **1**, by 4-(methoxycarbonyl)phenyl or 3-pyridyl groups at position 5 and by *N*-ethylcarboxamido or ethylaminomethyl groups at position 9 were investigated to explore potential additional interactions nearby the PAS. Despite some significant inter-species differences, the substitution pattern leading to a higher inhibitory activity both in EeAChE and hAChE involves the presence of a debenzylated nitrogen atom at position 1, and 4-chlorophenyl and *N*-ethylcarboxamido groups at positions 5 and 9, respectively. Overall, the hit-to-lead optimization process from **1** to **16a** simply involves a double bioisosteric O → NH replacement at position 1 and in the side chain at position 9, but results in a dramatic increase in EeAChE (>217-fold) and hAChE (>154-fold) inhibitory activities. Interestingly, such a change also leads to a noticeable increase in hBChE inhibitory activity (>11-fold). Because most AChE PAS inhibitors exhibit potencies in the micromolar range, the very potent hAChE inhibitory activity of the lead

16a (IC_{50} = 65 nM) might arise from additional interactions other than those established with PAS residues, as supported by the results derived from a comprehensive mechanistic study. On the one hand, kinetic studies and propidium displacement studies have confirmed the ability of **16a** to tightly bind the AChE PAS. On the other hand, molecular modelling studies have suggested the ability of the heteroaromatic system of **16a** to establish cation-π and π-π interactions with the PAS residue Trp286 but also the ability of the amide functionality at position 9 to penetrate along the gorge towards the catalytic site and to establish additional hydrogen bond interactions with AChE midgorge residues. The tight binding of **16a** to the AChE PAS and the additional midgorge interactions seem to account for its very potent hAChE inhibitory activity. Overall, the potent dual hAChE and hBChE inhibitory activities of **16a** make it a very interesting anti-Alzheimer lead compound.

4. Experimental part

4.1. Chemistry. General methods.

Melting points were determined in open capillary tubes with a MFB 595010M Gallenkamp melting point apparatus. 400 MHz ^{1}H/100.6 MHz ^{13}C NMR spectra were recorded on a Varian Mercury 400 spectrometer. The chemical shifts are reported in ppm (δ scale) relative to internal tetramethylsilane, and coupling constants are reported in Hertz (Hz). Assignments given for the NMR spectra of the new compounds have been carried out by comparison with the NMR data of **9c, 10c**, **11a**, **17a**, and **18b**, which in turn, were assigned on the basis of DEPT, COSY $^{1}H/^{1}H$ (standard procedures), and COSY $^{1}H/^{13}C$ (gHSQC or gHMBC sequences) experiments. IR spectra were run on a Perkin-Elmer Spectrum RX I or on a Thermo Nicolet Nexus spectrophotometer. Absorption values are expressed as wave-numbers (cm^{-1}); only significant absorption bands are given. Column chromatography was performed on silica gel 60 AC.C (35–70 mesh, SDS, ref 2000027). Thin-layer chromatography was performed with aluminum-backed sheets with silica gel 60 F_{254} (Merck, ref 1.05554), and spots were visualized with UV light and 1% aqueous solution of $KMnO_4$. NMR spectra of all of the new compounds were performed at the Centres Científics i Tecnològics of the University of Barcelona (CCiTUB), while elemental analyses and high resolution mass spectra were carried out at the Mycroanalysis Service of the IIQAB (CSIC, Barcelona, Spain) with a Carlo Erba model 1106 analyzer, and at the CCiTUB with a LC/MSD TOF Agilent

Technologies spectrometer, respectively. The HPLC measurements were performed using a HPLC Waters Alliance HT apparatus comprising a pump (Edwards RV12) with degasser, an autosampler, a diode array detector and a column as specified below. The reverse phase HPLC determinations were carried out on a YMC-Pack ODS-AQ column (50×4.6 mm, D S. 3 μm, 12 nm). Solvent A: water with 0.1% formic acid; Solvent B: acetonitrile with 0.1% formic acid. Gradient: 5% of B to 100% of B within 3.5 min. Flux: 1.6 mL/min at 50 ºC. The analytical samples of all of the compounds that were subjected to pharmacological evaluation were dried at 65 ºC / 2 Torr (standard conditions) and possess a purity ≥95% as evidenced by their elemental analyses and/or HPLC measurements. The synthetic procedures for the preparation of the intermediate and target compounds are exemplified through the synthesis of the most potent compound of the series, **16a**. The synthesis of the rest of compounds is included in the Supplementary Material.

*4.1.1. Ethyl 1-(tert-butoxycarbonyl)-5-(4-chlorophenyl)-1,2,3,4,4a,5,6,10b-octahydrobenzo[h][1,6]naphthyridine-9-carboxylate, diastereomeric mixture **8a***

To a stirred solution of *p*-chlorobenzaldehyde, **4a** (1.36 g, 9.67 mmol) and ethyl 4-aminobenzoate, (1.60 g, 9.69 mmol) in anhydrous CH_3CN (25 mL), 4 Å molecular sieves and $Sc(OTf)_3$ (0.95 g, 1.93 mmol) were added. The mixture was stirred at room temperature under argon atmosphere for 5 min and then treated with a solution of enamine **7** (1.80 mL, 1.78 g, 9.70 mmol) in anhydrous CH_3CN (12 mL). The resulting suspension was stirred at room temperature under argon atmosphere for 3 days. Then, the resulting mixture was diluted with sat. aq. $NaHCO_3$ (150 mL) and extracted with EtOAc (3 × 200 mL). The combined organic extracts were dried over anhydrous Na_2SO_4, filtered and evaporated under reduced pressure to give a solid residue (4.75 g), which was purified by column chromatography (35–70 μm silica gel, hexane/EtOAc mixtures, gradient elution). On elution with hexane/EtOAc 80:20 to 70:30, the diastereomeric mixture **8a** (2.86 g, 63% yield, 3:1 diastereomeric ratio (^{1}H NMR)) was isolated as a white solid.

*4.1.2. Ethyl 1-(tert-butoxycarbonyl)-5-(4-chlorophenyl)-1,2,3,4-tetrahydrobenzo[h][1,6]naphthyridine-9-carboxylate **11a***

To a solution of diastereomeric mixture **8a** (1.41 g, 2.99 mmol) in anhydrous $CHCl_3$ (37 mL), DDQ (1.36 g, 5.99 mmol) was added. The reaction mixture was stirred at room

temperature under argon atmosphere overnight, diluted with CH_2Cl_2 (150 mL) and washed with sat. aq. $NaHCO_3$ (3 × 200 mL). The combined organic extracts were dried over anhydrous Na_2SO_4, filtered and evaporated under reduced pressure to give an orange solid residue (1.46 g), which was purified through column chromatography (35–70 μm silica gel, hexane/EtOAc mixtures, gradient elution). On elution with hexane/EtOAc 80:20, compound **11a** (1.25 g, 90% yield) was isolated as a white solid; R_f 0.61 (hexane/EtOAc 1:1).

A solution of **11a** (100 mg, 0.21 mmol) in CH_2Cl_2 (8 mL) was filtered through a 0.2 μm PTFE filter and evaporated at reduced pressure. The solid was washed with pentane (3 × 4 mL) to give, after drying under standard conditions, the analytical sample of **11a** (97 mg): mp 154–155 °C (CH_2Cl_2); IR (KBr) *ν* 1713, 1697 (C=O st), 1618, 1592, 1577, 1566 (Ar–C–C and Ar–C–N st) cm^{-1}; ^1H NMR (400 MHz, $CDCl_3$) *δ* 1.39 [s, 9H, $C(CH_3)_3$], 1.43 (t, *J*=7.2 Hz, 3H, $CO_2CH_2CH_3$), 2.00 (br signal, 2H, 3-H_2), 2.80 (m, 2H, 4-H_2), 3.20–3.60 (br signal, 2H, 2-H_2), 4.45 (q, *J*=7.2 Hz, 2H, $CO_2CH_2CH_3$), 7.48 [ddd, *J*=8.4 Hz, *J'*≈*J''*≈2.0 Hz, 2H, 5–Ar–C3(5)-H], 7.55 [ddd, *J*≈8.4 Hz, *J'*≈*J''*≈2.0 Hz, 2H, 5–Ar–C2(6)-H], 8.08 (d, *J*≈8.8 Hz, 1H, 7-H), 8.24 (dd, *J*=8.8 Hz, *J'*=1.6 Hz 1H, 8-H), 8.59 (d, *J*=1.6 Hz, 1H, 10-H); ^{13}C NMR (100.6 MHz, $CDCl_3$) *δ* 14.3 (CH_3, $CO_2CH_2CH_3$), 24.1 (CH_2, C3), 25.4 (CH_2, C4), 27.9 [$3CH_3$, $C(CH_3)_3$], 44.7 (CH_2, C2), 61.3 (CH_2, $CO_2CH_2CH_3$), 82.1 [C, $C(CH_3)_3$], 122.9 (C, C10a), 123.8 (C, C4a), 127.0 (C, C9), 127.6 (CH, C10), 128.2 (CH, C8), 128.6 [2CH, 5–Ar–*C*3(5)], 129.7 (CH, C7), 130.3 [2CH, 5–Ar–*C*2(6)], 134.8 (C, 5–Ar–*C*4), 138.3 (C, 5–Ar–*C*1), 145.7 (C, C10b), 148.8 (C, C6a), 153.9 (C, NCOO), 160.5 (C, C5), 166.3 (C, $CO_2CH_2CH_3$); HRMS (ESI), calcd for [$C_{26}H_{27}{}^{35}ClN_2O_4 + H^+$] 467.1732, found 467.1723.

4.1.3. 1-(tert-butoxycarbonyl)-5-(4-chlorophenyl)-N-ethyl-1,2,3,4-tetrahydrobenzo[h][1,6]naphthyridine-9-carboxamide ***15a***

A suspension of ester **11a** (2.54 g, 5.44 mmol) and KOH (85% purity, 1.08 g, 16.3 mmol) in MeOH (140 mL) was stirred under reflux for 24 h. The resulting solution was cooled down at room temperature and concentrated under reduced pressure. The solid residue (3.35 g) was treated with a solution of HCl in Et_2O (0.8 N, 138 mL, 110 mmol) and the resulting suspension was concentrated under reduced pressure to give the corresponding aminoquinolino carboxylic acid, in the form of hydrochloride, as a white solid (3.77 g). This crude product was used in the next step without further purification.

A solution of this crude product (3.60 g) in anhydrous CH_2Cl_2 (45 mL) was cooled to 0º C with an ice bath and treated dropwise with freshly distilled Et_3N (2.89 mL, 2.10 g, 20.7 mmol) and $ClCO_2Et$ (0.49 mL, 556 mg, 5.12 mmol). The resulting suspension was thoroughly stirred at 0 º C for 30 min and treated with $EtNH_2 \cdot HCl$ (0.42 g, 5.15 mmol). The reaction mixture was stirred at room temperature for 3 days, diluted with 10% aq. Na_2CO_3 (200 mL), and extracted with CH_2Cl_2 (3 × 300 mL). The combined organic extracts were washed with H_2O (3 × 200 mL), dried over anhydrous Na_2SO_4, filtered and concentrated under reduced pressure to give a solid residue (2.36 g), which was purified through column chromatography (35-70 μm silica gel, hexane/EtOAc mixtures, gradient elution). On elution with hexane/EtOAc 60:40, amide **15a** (1.22 g, 50% overall yield) was obtained as a white solid; R_f 0.23 (hexane/EtOAc 1:1).

A solution of **15a** (50 mg, 0.11 mmol) in CH_2Cl_2 (4 mL) was filtered through a 0.2 μm PTFE filter and evaporated at reduced pressure. The solid was washed with pentane (3 × 4 mL) to give, after drying under standard conditions, the analytical sample of **15a** (45 mg) as a white solid: mp 203–204 °C (CH_2Cl_2); IR (ATR) ν 3391, 3316 (NH st), 1711, 1687, 1654, 1639, 1617, 1597, 1583, 1568, 1532 (C=O, Ar–C–C and Ar–C–N st) cm^{-1}; ^1H NMR (400 MHz, $CDCl_3$) δ 1.27 (t, J=7.2 Hz, 3H, $CONHCH_2CH_3$), 1.40 [s, 9H, $C(CH_3)_3$], 1.99 (br signal, 2H, 3-H_2), 2.79 (t, J=6.4 Hz, 2H, 4-H_2), 3.10–3.50 (br signal, 2H, 2-H_2), 3.54 (tt, J=7.2 Hz, J'≈5.2 Hz, 2H, $CONHCH_2CH_3$), 6.27 (t, J=5.2 Hz, 1H, $CONHCH_2CH_3$), 7.47 [ddd, J=8.4 Hz, J'≈J''≈2.0 Hz, 2H, 5–Ar–C3(5)-H], 7.53 [ddd, J≈8.4 Hz, J'≈J''≈2.0 Hz, 2H, 5–Ar–C2(6)-H], 7.96 (dd, J=8.4 Hz, J'=2.0 Hz, 1H, 8-H), 8.08 (d, J≈8.4 Hz, 1H, 7-H), 8.25 (br s, 1H, 10-H); ^{13}C NMR (100.6 MHz, $CDCl_3$) δ 14.9 (CH_3, $CONHCH_2CH_3$), 24.0 (CH_2, C3), 25.4 (CH_2, C4), 28.0 [$3CH_3$, $C(CH_3)_3$], 35.1 (CH_2, $CONHCH_2CH_3$), 44.8 (CH_2, C2), 82.1 [C, $C(CH_3)_3$], 123.0 (C, C10a), 124.0 (C, C4a), 124.2 (CH), 126.3 (CH) (C8 and C10), 128.6 [2CH, 5–Ar–C3(5)], 129.9 (CH, C7), 130.3 [2CH, 5–Ar–C2(6)], 131.4 (C, C9), 134.7 (C, 5–Ar–C4), 138.3 (C, 5–Ar–C1), 145.4 (C, C10b), 148.0 (C, C6a), 154.0 (C, NCOO), 159.9 (C, C5), 167.0 (C, $CONHCH_2CH_3$); HRMS (ESI), calcd for [$C_{26}H_{28}{}^{35}ClN_3O_3 + H^+$] 466.1892, found 466.1887.

*4.1.4. N-{{5-(4-chlorophenyl)-1,2,3,4-tetrahydrobenzo[h][1,6]naphthyridin-9-yl}methyl}ethanamine **18a** and 5-(4-chlorophenyl)-N-ethyl-1,2,3,4-tetrahydrobenzo[h][1,6]naphthyridine-9-carboxamide **16a***

A solution of amide **15a** (0.65 g, 1.39 mmol) in anhydrous THF (32 mL) was cooled to 0 ºC with an ice bath, and treated portionwise with $LiAlH_4$ (0.17 g, 4.48 mmol). The resulting suspension was stirred under reflux overnight, cooled to 0 ºC with an ice bath and treated dropwise with 1N NaOH (20 mL), then diluted with H_2O (25 mL), and extracted with EtOAc (3 × 30 mL). The combined organic extracts were dried over anhydrous Na_2SO_4, filtered and evaporated under reduced pressure to give a solid residue (0.51 g), which was purified through column chromatography (35-70 μm silica gel, CH_2Cl_2/MeOH/50% aq. NH_4OH mixtures, gradient elution). On elution with CH_2Cl_2/MeOH/50% aq. NH_4OH 99:1:0.2, *N*-Boc-deprotected amide **16a** (72 mg, 14% yield) was isolated as a yellowish solid. On elution with CH_2Cl_2/MeOH/50% aq. NH_4OH 97:3:0.2 to 95:5:0.2, *N*-Boc-deprotected amine **18a** (170 mg, 35% yield) was isolated as a yellowish solid; $R_{f(\mathbf{16a})}$ 0.15 (CH_2Cl_2 /MeOH/NH_4OH 9:1:0.05); $R_{f(\mathbf{18a})}$ 0.49 (CH_2Cl_2 /MeOH/NH_4OH 9:1:0.05).

A solution of **16a** (64 mg, 0.17 mmol) in CH_2Cl_2 (5 mL) was filtered through a 0.2 μm PTFE filter and treated with a methanolic solution of HCl (0.75 N, 2.2 mL, 1.65 mmol). The resulting solution was evaporated at reduced pressure and the solid was washed with pentane (3 × 4 mL) to give, after drying under standard conditions, **16a**·HCl (57 mg) as a brown solid: mp 320–321 ºC (CH_2Cl_2 /MeOH 69:31); IR (ATR) ν 3500–2500 (max at 3395, 3231, 3090, 3028, 2929, 2865, 2810, 2640, $^+$NH, NH, OH and CH st), 1655, 1647, 1629, 1586, 1545 (C=O, Ar–C–C and Ar–C–N st) cm^{-1}; ^{1}H NMR (400 MHz, CD_3OD) δ 1.29 (t, J=7.2 Hz, 3H, $CONHCH_2CH_3$), 1.99 (tt, $J \approx J' \approx 6.0$ Hz, 2H, 3-H_2), 2.75 (t, $J \approx 6.0$ Hz, 2H, 4-H_2), 3.49 (q, J=7.2 Hz, 2H, $CONHCH_2CH_3$), 3.71 (t, J=5.6 Hz, 2H, 2-H_2), 4.84 (s, NH and $^+$NH), 7.66 [complex signal, 4H, 5–Ar–C2(6)-H and 5–Ar–C3(5)-H], 7.85 (d, $J \approx 9.2$ Hz, 1H, 7-H), 8.24 (dd, J=9.2 Hz, J'=1.6 Hz, 1H, 8-H), 8.86 (d, J=1.6 Hz, 1H, 10-H); ^{13}C NMR (100.6 MHz, CD_3OD) δ 14.8 (CH_3, $CONHCH_2CH_3$), 20.0 (CH_2, C3), 25.0 (CH_2, C4), 36.2 (CH_2, $CONHCH_2CH_3$), 43.0 (CH_2, C2), 109.8 (C, C4a), 116.2 (C, C10a), 120.9 (CH, C7), 123.6 (CH, C10), 130.4 (2CH), 131.8 (2CH) [5–Ar–*C*2(6) and 5–Ar–*C*3(5)], 132.3 (C, 5–Ar–*C*1), 132.5 (CH, C8), 133.8 (C, C9), 138.3 (C, 5–Ar–*C*4), 140.2 (C, C6a), 151.5 (C, C5), 155.8 (C, C10b), 168.1 (C, $CONHCH_2CH_3$); HRMS (ESI), calcd for [$C_{21}H_{20}{}^{35}ClN_3O + H^+$] 366.1368, found 366.1364; Elemental analysis, calcd for $C_{21}H_{20}ClN_3O \cdot HCl \cdot H_2O$ C 60.01%, H 5.52%, N 10.00%, Cl 16.87%, found C 60.35%, H 5.81%, N 8.93%, Cl 16.05%. HPLC purity: 94%.

A solution of **18a** (106 mg, 0.30 mmol) in CH_2Cl_2 (8 mL) was filtered through a 0.2 μm PTFE filter and treated with a methanolic solution of HCl (0.75 N, 3.6 mL, 2.70 mmol). The resulting solution was evaporated at reduced pressure and the solid was washed with pentane (3 × 4 mL) to give, after drying under standard conditions, **18a**·2HCl (96 mg) as a yellowish solid: mp 323–324 ºC (CH_2Cl_2/MeOH 69:31); IR (KBr) *ν* 3500–2400 (max at 3379, 3198, 3095, 3028, 2926, 2863, 2767, 2667, 2552, 2422, $^+$NH, NH and CH st), 1639, 1587, 1504 (Ar–C–C and Ar–C–N st) cm^{-1}; ^{1}H NMR (400 MHz, CD_3OD) *δ* 1.41 (t, *J*=7.6 Hz, 3H, 9-$CH_2NHCH_2CH_3$), 1.99 (tt, *J*≈*J'*≈6.0 Hz, 2H, 3-H_2), 2.76 (t, *J*=6.0 Hz, 2H, 4-H_2), 3.23 (q, *J*=7.6 Hz, 2H, 9-$CH_2NHCH_2CH_3$), 3.73 (t, *J*=5.6 Hz, 2H, 2-H_2), 4.44 (s, 2H, 9-$CH_2NHCH_2CH_3$), 4.84 (s, NH and $^+$NH), 7.67 [complex signal, 4H, 5–Ar–C2(6)-H and 5–Ar–C3(5)-H], 7.92 (d, *J*=8.8 Hz, 1H, 7-H), 8.06 (dd, *J*=8.8 Hz, *J'*=1.6 Hz, 1H, 8-H), 8.58 (d, *J*=1.6 Hz, 1H, 10-H); ^{13}C NMR (100.6 MHz, CD_3OD) *δ* 11.6 (CH_3, 9-$CH_2NHCH_2CH_3$), 20.0 (CH_2, C3), 25.1 (CH_2, C4), 43.0 (CH_2, C2), 44.2 (CH_2, 9-$CH_2NHCH_2CH_3$), 51.5 (CH_2, 9-$CH_2NHCH_2CH_3$), 109.8 (C, C4a), 116.7 (C, C10a), 121.7 (CH, C7), 126.0 (CH, C10), 130.4 (2CH), 131.8 (2CH) [5–Ar–*C*2(6) and 5–Ar–*C*3(5)], 131.0 (C, C9), 132.3 (C, 5–Ar–*C*1), 135.5 (CH, C8), 138.2 (C, 5–Ar–*C*4), 139.1 (C, C6a), 151.4 (C, C5), 155.2 (C, C10b); HRMS (ESI) calcd for [$C_{21}H_{22}{}^{35}ClN_3 + H^+$] 352.1575, found 352.1574; Elemental analysis, calcd for $C_{21}H_{22}ClN_3$·1.5HCl·2.75H_2O C 55.30%, H 6.41%, N 9.21%, Cl 19.43%, found C 55.23%, H 6.16%, N 8.93%, Cl 19.10%. HPLC purity > 99%.

4.2. Biological assays

4.2.1. Determination of inhibitory effect on AChE and BChE activity

The inhibitory activity against *Electrophorus electricus* (Ee) AChE (Sigma-Aldrich) and human serum BChE (Sigma-Aldrich) was evaluated spectrophotometrically by the method of Ellman *et al.* [15]. The reactions took place in a final volume of 300 μL of 0.1 M phosphate-buffered solution pH 8.0, containing EeAChE (0.03 u/mL) or hBChE (0.02 u/mL) and 333 μM 5,5'-dithiobis(2-nitrobenzoic) acid (DTNB; Sigma-Aldrich) solution used to produce the yellow anion of 5-thio-2-nitrobenzoic acid. Inhibition curves were performed in duplicates using at least 10 increasing concentrations of inhibitors and preincubated for 20 min at 37 ºC before adding the substrate [28]. One duplicate sample without inhibitor was always present to yield 100% of AChE or BChE activities. Then substrates, acetylthiocholine iodide (450 μM; Sigma-Aldrich) or

butyrylthiocholine iodide (300 μM; Sigma-Aldrich), were added and the reaction was developed for 5 min at 37 ºC. The colour production was measured at 414 nm using a labsystems Multiskan spectrophotometer.

Data from concentration−inhibition experiments of the inhibitors were calculated by non-linear regression analysis, using the GraphPad Prism program package (GraphPad Software; San Diego, USA), which gave estimates of the IC_{50} (concentration of drug producing 50% of enzyme activity inhibition). Results are expressed as mean ± S.E.M. of at least 4 experiments performed in duplicate.

The inhibitory activity against human recombinant AChE was also assessed using the method of Ellman *et al.* [15]. Initial rate assays were performed at 37 °C with a Jasco V-530 double beam Spectrophotometer. The rate of increase in the absorbance at 412 nm was followed for 240 s. AChE stock solution was prepared by dissolving human recombinant AChE (E.C.3.1.1.7) lyophilized powder (Sigma-Aldrich) in 0.1 M phosphate buffer (pH = 8.0) containing Triton X-100 0.1%. Stock solutions of inhibitors (1-3 mM) were prepared in methanol and diluted in methanol. Inhibitors were first screened at a single concentration (25 μM). Then, for compounds showing a percentage of inhibition higher than 50% at the screening concentration (25 μM), the IC_{50} values were determined. In this case, five/six increasing concentrations of the inhibitor were used, able to give an inhibition of the enzymatic activity in the range of 20-80%. The assay solution consisted of a 0.1 M phosphate buffer pH 8.0, with the addition of 340 μM DTNB, 0.02 unit/mL of human recombinant AChE and 550 μM of substrate (acetylthiocholine iodide, ATCh). 50 μL aliquots of increasing concentration of the tested inhibitor (or methanol) were added to the assay solution and pre-incubated with the enzyme for 20 min at 37 °C before the addition of the substrate. Assays were carried out with a blank containing all components except AChE in order to account for the non-enzymatic hydrolysis of the substrate. The reaction rates were compared and the percent inhibition due to the presence of inhibitor was calculated. Each concentration was analyzed in duplicate, and IC_{50} values were determined graphically from log concentration–inhibition curves (GraphPad Prism 4.03 software, GraphPad Software Inc.). Two/three independent experiments were performed for the determination of each IC_{50} value.

4.2.2. Kinetic inhibition studies

To estimate the mode of inhibition of compound **16a** and the corresponded benzylated analogue **14a**, Lineweaver-Burk double reciprocal plots were constructed at relatively low concentration of substrate (0.11–0.55 mM) and using the same experimental conditions reported for the hAChE assay at section *4.2.1*. The plots were assessed by a weighted least square analysis that assumed the variance of v to be a constant percentage of v for the entire data set. To confirm the mode of inhibition, Cornish-Bowden plots were obtained by plotting S/v (substrate/velocity ratio) *versus* inhibitor concentration [21]. Data analysis was performed with GraphPad Prism 4.03 software (GraphPad Software Inc.).

Calculation of the inhibitor constant (K_i) value was carried out by re-plotting slopes of lines from the Lineweaver-Burk plot *versus* the inhibitor concentration and K_i was determined as the intersect on the negative x-axis. K'_i (dissociation constant for the enzyme-substrate-inhibitor complex) value was determined by plotting the apparent 1/ $v_{max,\ app}$ *versus* inhibitor concentration [29].

4.2.3. Propidium displacement studies

The affinity of selected inhibitors for the peripheral binding site of EeAChE (type VI-S, Sigma-Aldrich) was tested using propidium iodide (P) (Sigma-Aldrich), a known PAS-specific ligand as previously described by Taylor *et al.* [22]. A shift in the excitation wavelength follows the complexation of propidium iodide and AChE [22a]. Fluorescence intensity was monitored by a Jasco 6200 spectrofluorometer (Jasco Europe, Italy) using a 0.5 mL quartz cuvette at room temperature. EeAChE (2 μM, assuming 82,000 molecular mass subunits) was first incubated with 8 μM propidium iodide in 1 mM Tris-HCl, pH 8.0 at room temperature. Stock solutions (4 mM) of each inhibitor were prepared in methanol. In the back titration experiments of the propidium-AChE complex by the tested inhibitor, aliquots of inhibitor (2-40 μM, 4-68 μM and 2-44 μM for **16a**, **18a** and **14a**, respectively) were added successively, and fluorescence emission was monitored at 602 nm upon excitation at 535 nm. Blanks containing propidium alone, inhibitor plus propidium and EeAChE alone were prepared and fluorescence emission determined. Raw data were processed following the method of Taylor and Lappi [22b] to estimate K_D values assuming a dissociation constant value for propidium for acetylcholinesterase from *Electrophorus electricus* equals to 0.7 μM [23].

4.2.4. PAMPA-BBB assay

To evaluate the brain penetration of the synthesized compounds, a parallel artificial membrane permeation assay for blood-brain barrier was used, following the method described by Di *et al.* [27]. The *in vitro* permeability (P_e) of fourteen commercial drugs through lipid extract of porcine brain membrane together with the test compounds was determined. Commercial drugs and the synthesized compounds were tested using a mixture of PBS:EtOH (70:30). Assay validation was made by comparing the experimental permeability of the different compounds with the reported bibliography values of the commercial drugs, which showed a good correlation: P_e (exp) = 1.4974 P_e (lit) – 0.8434 (R^2 = 0.9428). From this equation and taking into account the limits established by Di *et al.* for BBB permeation, we established the ranges of permeability as compounds of high BBB permeation (CNS+): P_e (10^{-6} cm s^{-1}) > 5.1; compounds of low BBB permeation (CNS–): P_e (10^{-6} cm s^{-1}) < 2.15, and compounds of uncertain BBB permeation (CNS+/–): 5.1 > P_e (10^{-6} cm s^{-1}) > 2.15.

4.3. Molecular modelling

4.3.1. Setup of the system

Molecular modelling was performed using the X-ray crystallographic structure of the recombinant human AChE (PDB ID: 3LII) [30]. The structure was refined by removal of *N*-acetyl-D-glucosamine and sulfate anions and addition of missing hydrogen atoms. Furthermore, the missing loop that comprises residues 259-263 (PGGTG) was modeled from the X-ray structure of hAChE complexed with huprine W (PDB ID: 4BDT) [31]. The enzyme was modeled in its physiological active form with neutral His447 and deprotonated Glu334, which together with Ser203 form the catalytic triad. The ionization state for the rest of ionizable residues was assessed from PROPKA3 calculations [32]. Accordingly, the standard ionization state at neutral pH was considered but for residues Glu285, Glu450 and Glu452, which were protonated. Finally, three disulfide bridges were defined between Cys residues 257-272, 529-409, and 69-96, respectively. Structural waters were retrieved from those found in the AChE-donepezil complex 1EVE [33].

Since Trp286 can adopt three main conformations in the peripheral binding site [9], three models were built up by re-orienting the side chain of Trp 286 as found in the X-ray structures of the AChE complexes with propidium, *bis*(7)-tacrine and *syn*-TZ2PA6

(PDB ID: 1N5R, 2CKM and 1Q83, respectively). These models were energy minimized using the AMBER force field (see below).

4.3.2. Docking

Docking of AChE inhibitors was performed using the rDock program, which is an extension of the program RiboDock and utilizes an empirical scoring function calibrated on the basis of protein–ligand complexes [24]. It is worth noting that previous studies strongly support the excellent performance of rDock for predicting the binding mode of a variety of AChE inhibitors to the enzyme gorge [9]. A cavity of radius 17 Å, centered on the structure of a superligand containing huprine X, donepezil and propidium (as found in the X-ray structures 1E66 [34], 1EVE and 1N5R) was used to define the docking volume. Since huprine X and propidium are bound to the catalytic and peripheral binding sites, and donepezil is aligned along the gorge, this definition guarantees the exploration of the binding mode along the whole volume accessible for binding. Calculations were performed with no structural waters. Conformational flexibility around rotatable bonds of the ligand was allowed. Docking calculations were performed separately for the three models of the human enzyme, which differ in the relative orientation of the side chain of Trp286 (see above). Conformational adjustments of other residues in the binding site were accounted for indirectly by rescaling (by a factor of 0.9) the van der Waals volume of atoms. Each compound was subjected to 100 docking runs and the poses were sorted according to its docking score. The top 50 best scored poses were clustered and further analyzed by visual inspection.

4.3.3. Molecular dynamics simulations

Molecular dynamics (MD) simulations were run to further check the stability of the proposed binding mode of AChE inhibitors. Starting from the initial poses obtained from docking calculations, a 100 ns MD simulation was performed using the PMEMD module of AMBER12 [35] software package and the parm99SB [36] force field for the protein and GAFF [37]-derived parameters for the ligand. The geometry of the ligand was optimized at the B3LYP/6-31G(d) level [38]. The charge distribution of the inhibitors was defined from the electrostatic charges determined by fitting the B3LYP/6-31G(d) electrostatic potential using the RESP procedure [39]. Na^+ cations were added to neutralize the negative charge of the system with the XLEAP module of AMBER12. The system was immersed in an octahedral box of TIP3P water molecules

[40], preserving the crystallographic waters inside the binding cavity. The final system contained around 53,000 atoms.

The geometry of the system was minimized in four steps. First, water molecules and counterions were refined through 7000 steps of conjugate gradient and 3000 steps of steepest descent algorithm. Then, the position of hydrogen atoms was optimized using 4500 steps of conjugate gradient and 500 steps of steepest descent algorithm. At the third stage, hydrogen atoms, water molecules and counterions were further optimized using 11500 steps of conjugate gradient and 3500 steps of steepest descent algorithm. Finally, the whole system was optimized using 8500 steps of conjugate gradient and 2500 steps of steepest descent algorithm. Thermalization of the system was performed in five steps of 25 ps, increasing the temperature from 50 to 298 K. Concomitantly, the residues that define the binding site were restrained during thermalization using a variable restraining force. Thus, a force costant of 25 $kcal \cdot mol^{-1} \cdot Å^{-2}$ was used in the first stage of the thermalization and was subsequently decreased by increments of 5 $kcal \cdot mol^{-1} \cdot Å^{-2}$ in the next stages. Then, an additional step of 250 ps was performed in order to equilibrate the system density at constant pressure (1 bar) and temperature (298 K). Finally, a 100 ns trajectory was run using a time step of 2 fs. SHAKE was used for those bonds containing hydrogen atoms in conjunction with periodic boundary conditions at constant volume and temperature, particle mesh Ewald for the treatment of long range electrostatic interactions, and a cutoff of 10 Å for nonbonded interactions. The structural analysis was performed using in-house software and standard codes of AMBER12. The solvent interaction energies (SIE) technique developed by Purisima and co-workers was used to estimate the interaction free energies for the AChE inhibitors [26]. Calculations were performed for a set of 150 snapshots taken along the last 30 ns of the MD trajectory.

Acknowledgments

This work was supported by Ministerio de Ciencia e Innovación (MICINN) (CTQ2011-22433, CTQ2012-30930, SAF2011-27642, SAF2009-10553) and Generalitat de Catalunya (GC) (2009SGR1396, 2009SGR1024, 2009SGR249). This work was supported by MIUR (PRIN 2009Z8YTYC-003. Fellowship from GC to E.V. and from Leonardo da Vinci Project Unipharma-Graduates 6 to O.D.P. are gratefully acknowledged. The Center for Scientific and Academic Services of Catalonia (CESCA) is acknowledged for providing access to computational facilities. We thank Dr. Marc

Revés (Universitat de Barcelona) for his helpful assistance in the HPLC purity measurements.

Appendix A. Supplementary material

Supplementary data related to this article can be found at http://dx.doi.org/. These data include synthetic procedures and chemical characterization data of compounds **6a**–**c**, **8b**, **9a**–**c**, **10a**–**c**, **11b**, **12a**,**b**, **13a**, **14a**, **16b**, **17a**, and **18b**, additional results from the molecular modeling studies and PAMPA-BBB assay, as well as copies of the ^{1}H and ^{13}C NMR spectra and HPLC chromatograms of the tested compounds.

References

[1] N.L. Batsch, M.S. Mittelman, World Alzheimer Report 2012. Overcoming the stigma of dementia, London: Alzheimer's Disease International, 2012 (http://www.alz.co.uk).

[2] Alzheimer's Association, 2013 Alzheimer's disease facts and figures, Alzheimers Dementia 9 (2013) 208–245.

[3] S.W. Pimplikar, Reassessing the amyloid cascade hypothesis of Alzheimer's disease, Int. J. Biochem. Cell Biol. 41 (2009) 1261–1268.

[4] (a) W.J. Geldenhuys, C.J. Van der Schyf, Rationally designed multi-targeted agents against neurodegenerative diseases, Curr. Med. Chem. 20 (2013) 1662–1672;

(b) X. Chen, M. Decker, Multi-target compounds acting in the central nervous system designed from natural products, Curr. Med. Chem. 20 (2013) 1673–1685;

(c) P. Russo, A. Frustaci, A. Del Bufalo, M. Fini, A. Cesario, Multitarget drugs of plants origin acting on Alzheimer's disease, Curr. Med. Chem. 20 (2013) 1686–1693;

(d) A. Rampa, F. Belluti, S. Gobbi, A. Bisi, Hybrid-based multi-target ligands for the treatment of Alzheimer's disease, Curr. Top. Med. Chem. 11 (2011) 2716-2730;

(e) A. Cavalli,; M.L. Bolognesi, A. Minarini, M. Rosini, V. Tumiatti, M. Recanatini, C. Melchiorre, Multi-target-directed ligands to combat neurodegenerative diseases, J. Med. Chem. 51 (2008) 347–372.

[5] (a) R.A. Sperling, J. Karlawish, K.A. Johnson, Preclinical Alzheimer disease – the challenges ahead, Nat. Rev. Neurol. 9 (2013) 54–58;
(b) D.C. Anderson, Alzheimer's disease biomarkers: More than molecular diagnostics, Drug Dev. Res. 74 (2013) 92–111;
(c) S.J. Teipel, O. Sabri, M. Grothe, H. Barthel, D. Prvulovic, K. Buerger, A.L. Bokde, M. Ewers, W. Hoffmann, H. Hampel, Perspectives for multimodal neurochemical and imaging biomarkers in Alzheimer's disease, J. Alzheimers Dis. 33(Suppl. 1) (2013) S329–S347;
(d) J.F. Quinn, Biomarkers for Alzheimer's disease; showing the way or leading us astray?, J. Alzheimers Dis. 33 (Suppl. 1) (2013) S371–S376;
(e) R.J. Caselli, E.M. Reiman, Characterizing the preclinical stages of Alzheimer's disease and the prospect of presymptomatic intervention, J. Alzheimers Dis. 33 (Suppl. 1) (2013) S405–S416;
(f) V.T. Papaliagkas, The role of cerebrospinal fluid biomarkers for Alzheimer's disease diagnosis. Where are we now?, Recent Patents CNS Drug Discov. 8 (2013) 70–78.

[6] (a) L. Cheewakriengkrai, S. Gauthier, A 10-year perspective on donepezil, Expert Opin. Pharmacother. 14 (2013) 331–338;
(b) J.L. Cummings, S.J. Banks, R.K. Gary, J.W. Kinney, J.M. Lombardo, R.R. Walsh, K. Zhong, Alzheimer's disease drug development: translational neuroscience strategies, CNS Spectr. 18 (2013) 128–138;
(c) M.B. Colovic, D.Z. Krstic, T.D. Lazarevic-Pasti, A.M. Bondzic, V.M. Vasic, Acetylcholinesterase inhibitors: pharmacology and toxicology, Curr. Neuropharmacol. 11 (2013) 315–335;
(d) P. Anand, B. Singh, A review on cholinesterase inhibitors for Alzheimer's disease, Arch. Pharm. Res. 36 (2013) 375–399.

[7] J.L. Sussman, M. Harel, F. Frolow, C. Oefner, A. Goldman, L. Toker, I. Silman, Atomic structure of acetylcholinesterase from Torpedo californica – a prototypic acetylcholine-binding protein, Science 253 (1991) 872–879.

[8] (a) M.L. Bolognesi, A. Minarini, M. Rosini, V. Tumiatti, C. Melchiorre, From dual binding site acetylcholinesterase inhibitors to multi-target-directed ligands (MTDLs): a step forward in the treatment of Alzheimer's disease, Mini-Rev. Med. Chem. 8 (2008) 960–967;

(b) A. Castro, P. Muñoz, A. Martínez, Dual binding site acetylcholinesterase inhibitors: design, SAR, and potential role as new disease-modifying agents for Alzheimer's disease, in: A. Martínez Gil (Ed.), Medicinal Chemistry of Alzheimer's Disease, Transworld Research Network, Kerala, 2008, pp. 21–44;
(c) D. Muñoz-Torrero, Acetylcholinesterase inhibitors as disease-modifying therapies for Alzheimer's disease, Curr. Med. Chem. 15 (2008) 2433–2455.

[9] P. Camps, X. Formosa, C. Galdeano, D. Muñoz-Torrero, L. Ramírez, E. Gómez, N. Isambert, R. Lavilla, A. Badia, M.V. Clos, M. Bartolini, F. Mancini, V. Andrisano, M.P. Arce, M.I. Rodríguez-Franco, O. Huertas, T. Dafni, F.J. Luque, Pyrano[3,2-*c*]quinoline–6-chlorotacrine hybrids as a novel family of acetylcholinesterase- and β-amyloid-directed anti-Alzheimer compounds, J. Med. Chem. 52 (2009) 5365–5379.

[10] L.S. Povarov, α,β-Unsaturated ethers and their analogues in reactions of diene synthesis, Russ. Chem. Rev. 36 (1967) 656–670.

[11] (a) E. Vicente-García, F. Catti, R. Ramón, R. Lavilla, Unsaturated lactams: new inputs for Povarov-type multicomponent reactions, Org. Lett. 12 (2010) 860–863;
(b) D. A. Powell, R. A. Batey, Total synthesis of the alkaloids martinelline and martinellic acid via a hetero Diels−Alder multicomponent coupling reaction, Org. Lett. 4 (2002) 2913–2916.

[12] O. Jiménez, G. de la Rosa, R. Lavilla, Straightforward access to a structurally diverse set of oxacyclic scaffolds through a four-component reaction, Angew. Chem., Int. Ed. 44 (2005) 6521–6525.

[13] E. Vicente-García, R. Ramón, S. Preciado, R. Lavilla, Multicomponent reaction access to complex quinolines via oxidation of the Povarov adducts, Beilstein J. Org. Chem. 7 (2011) 980–987.

[14] S. Das, D. Addis, S. Zhou, K. Junge, M. Beller, Zinc-catalyzed reduction of amides: unprecedented selectivity and functional group tolerance, J. Am. Chem. Soc. 132 (2010) 1770–1771.

[15] G.L. Ellman, K.D. Courtney, V. Andres Jr., R.M. Featherstone, A new and rapid colorimetric determination of acetylcholinesterase activity, Biochem. Pharmacol. 7 (1961) 88–95.

[16] R.M. Lane, S.G. Potkin, A. Enz, Targeting acetylcholinesterase and butyrylcholinesterase in dementia, Int. J. Neuropsychopharmacol. 9 (2006) 101–124.

[17] C.D. Anderson, N. Forsgren, C. Akfur, A. Allgardsson, L. Berg, C. Engdahl, W. Qian, F.J. Ekström, A. Linusson, Divergent structure-activity relationships of structurally similar acetylcholinesterase inhibitors, J. Med. Chem. 56 (2013), 76151−7624.

[18] M.L. Bolognesi, V. Andrisano, M. Bartolini, R. Banzi, C. Melchiorre, Propidium-based polyamine ligands as potent inhibitors of acetylcholinesterase and acetylcholinesterase-induced amyloid-β aggregation, J. Med. Chem. 48 (2005) 24–27.

[19] E. Viayna, R. Sabate, D. Muñoz-Torrero, Dual inhibitors of β-amyloid aggregation and acetylcholinesterase as multi-target anti-Alzheimer drug candidates, Curr. Top. Med. Chem. 13 (2013) 1820–1842.

[20] (a) Z. Radić, P. Taylor, Interaction kinetics of reversible inhibitors and substrates with acetylcholinesterase and its fasciculin 2 complex, J. Biol. Chem. 276 (2001) 4622–4633;
(b) Y. Bourne, P. Taylor, Z. Radić, P. Marchot, Structural insights into ligand interactions at the acetylcholinesterase peripheral anionic site, Embo J. 22 (2003) 1–12;
(c) B. Kaboudin, S. Emadi, M.R. Faghihi, M. Fallahi, V. Sheik-Hasani, Synthesis of α-oxycarbanilinophosphonates and their anticholinesterase activities: the most potent derivative is bound to the peripheral site of acetylcholinesterase, J. Enzyme Inhib. Med. Chem. 28 (2013) 576–582;
(d) S. Young, K. Fabio, C. Guillon, P. Mohanta, T.A. Halton, D.E. Heck, R.A. Flowers II, J.D. Laskin, N.D. Heindel, Peripheral site acetylcholinesterase inhibitors targeting both inflammation and cholinergic dysfunction, Bioorg. Med. Chem. Lett. 20 (2010) 2987–2990;
(e) P. de la Torre, L. Astudillo Saavedra, J. Caballero, J. Quiroga, J.H. Alzate-Morales, M. Gutiérrez Cabrera, J. Trilleras, A novel class of selective acetylcholinesterase inhibitors: synthesis and evaluation of (*E*)-2-(benzo[*d*]thiazol-2-yl)-3-heteroarylacrylonitriles, Molecules 17 (2012) 12072–12085.

[21] A. Cornish-Bowden, A simple graphical method for determining the inhibition constants of mixed, uncompetitive and non-competitive inhibitors, Biochem. J. 137 (1974) 143–144.

[22] (a) P. Taylor, J. Lwebuga-Mukasa, S. Lappi, J. Rademacher, Propidium – a fluorescent probe for a peripheral anionic site on acetylcholinesterase, Mol. Pharmacol. 10 (1974) 703–708;
(b) P. Taylor, S. Lappi, Interaction of fluorescence probes with acetylcholinesterase, The site and specificity of propidium binding, Biochemistry 14 (1975) 1989–1997.

[23] N. Nunes-Tavares, A. Nery da Matta, C.M. Batista e Silva, G.M. Araújo, S.R. Louro, A. Hassón-Voloch, Inhibition of acetylcholinesterase from *Electrophorus electricus* (L.) by tricyclic antidepressants, Int. J. Biochem. Cell Biol. 34 (2002) 1071–1079.

[24] (a) S.D. Morley, M. Afshar, Validation of an empirical RNA-ligand scoring function for fast flexible docking using RiboDock, J. Comput.-Aided Mol. Des. 18 (2004) 189–208;
(b) X. Barril, R.E. Hubbard, S.D. Morley, Virtual screening in structure-based drug discovery, Mini-Rev. Med. Chem. 4 (2004) 779–791.

[25] C. Galdeano, E. Viayna, P. Arroyo, A. Bidon-Chanal, J.R. Blas, D. Muñoz-Torrero, F.J. Luque, Structural determinants of the multifunctional profile of dual binding site acetylcholinesterase inhibitors as anti-Alzheimer agents, Curr. Pharm. Design 16 (2010) 2818–2836.

[26] (a) M. Naïm, S. Bhat, K.N. Rankin, S. Dennis, S. F. Chowdhury, I. Siddiqi, P. Drabik, T. Sulea, C.I. Bayly, A. Jakalian, E.O. Purisima, Solvated interaction energy (SIE) for scoring protein−ligand binding affinities. 1. Exploring the parameter space, J. Chem. Inf. Model. 47 (2007) 122–133;
(b) Q. Cui, T. Sulea, J.D. Schrag, C. Munger, M.-N. Hung, M. Naïm, M. Cygler, E.O. Purisima, Molecular dynamics-solvated interaction energy studies of protein−protein interactions: the MP1-p14 scaffolding complex, J. Mol. Biol. 379 (2008) 787–802.

[27] L. Di, E.H. Kerns, K. Fan, O.J. McConnell, G.T. Carter, High throughput artificial membrane permeability assay for blood-brain barrier, Eur. J. Med. Chem. 38 (2003) 223–232.

[28] E. Viayna, T. Gómez, C. Galdeano, L. Ramírez, M. Ratia, A. Badia, M.V. Clos, E. Verdaguer, F. Junyent, A. Camins, M. Pallàs, M. Bartolini, F. Mancini, V. Andrisano, M.P. Arce, M.I. Rodríguez-Franco, A. Bidon-Chanal, F.J. Luque, P. Camps, D. Muñoz-Torrero, Novel huprine derivatives with inhibitory activity toward β-amyloid aggregation and formation as disease-modifying anti-Alzheimer drug candidates, ChemMedChem 5 (2010) 1855–1870.

[29] R.B. Silverman, The organic chemistry of enzyme-catalyzed reactions. Academic Press, San. Diego, 2000.

[30] H. Dvir, I. Silman, M. Harel, T.L. Rosenberry, J.L. Sussman. Acetylcholinesterase: from 3D structure to function. Chem. Biol. Interact. 187 (2010) 10–22.

[31] F. Nachon, E. Carletti, C. Ronco, M. Trovaslet, Y. Nicolet, L. Jean, P.-Y. Renard, Crystal structures of human cholinesterases in complex with huprine W and tacrine: elements of specificity for anti-Alzheimer's drugs targeting acetyl- and butyrylcholinesterase. Biochem. J. 453 (2013) 393–399.

[32] M.H.M. Olsson, C.R. Sondergard, M. Rostkowski, J.H. Jensen, PROPKA3: Consistent treatment of internal and surface residues in empirical pKa predictions. J. Chem. Theory Comput. 7 (2011) 525–537.

[33] G. Kryger, I. Silman, J.L. Sussman, Structure of acetylcholinesterase complexed with E2020 (Aricept): Implications for the design of new anti-Alzheimer drugs, Structure 7 (1999) 297–307.

[34] H. Dvir, D.M. Wong, M. Harel, X. Barril, M. Orozco, F.J. Luque, D. Muñoz-Torrero, P. Camps, T.L. Rosenberry, I. Silman, J.L. Sussman, 3D Structure of *Torpedo californica* acetylcholinesterase complexed with huprine X at 2.1 Å resolution: kinetic and molecular dynamics correlates, Biochemistry 41 (2002) 2970–2981.

[35] D.A. Case, T.A. Darden, T.E. Cheatham, III, C.L. Simmerling, J. Wang, R.E. Duke, R. Luo, R.C. Walker, W. Zhang, K.M. Merz, B. Roberts, S. Hayik, A. Roitberg, G. Seabra, J. Swails, A.W. Goetz, I. Kolossváry, K.F. Wong, F. Paesani, J. Vanicek, R.M. Wolf, J. Liu, X. Wu, S.R. Brozell, T. Steinbrecher, H. Gohlke, Q. Cai, X. Ye, J. Wang, M.-J. Hsieh, G. Cui, D.R. Roe, D.H. Mathews, M.G. Seetin, R. Salomon-Ferrer, C. Sagui, V. Babin, T. Luchko, S. Gusarov, A.

Kovalenko, P.A. Kollman (2012), *AMBER 12*, University of California, San Francisco.

[36] V. Hornak, R. Abel, A. Okur, B. Strockbine, A. Roitberg, C. Simmerling, Comparison of multiple Amber force fields and development of improved protein backbone parameters, Proteins 65 (2006), 712–725.

[37] J. Wang, R.M. Wolf, J.W. Caldwell, P.A. Kollman, D.A. Case, Development and testing of a general AMBER force field, J. Comput. Chem. 25 (2004) 1157–1174.

[38] (a) A.D. Becke, Density-functional thermochemistry. III. The role of exact exchange, J. Chem. Phys. 98 (1993) 5648–5652;
(b) C. Lee, W. Yang, R.G. Parr, Development of the Colle-Salvetti correlation-energy formula into a functional of the electron density, Phys. Rev. B 37 (1988) 785–789.

[39] C.I. Bayly, P. Cieplak, W.D. Cornell, P.A. Kollman, A well-behaved electrostatic potential based method using charge restraints for deriving atomic charges, J. Phys. Chem. 97 (1993) 10269–10280.

[40] W.L. Jorgensen, J. Chandrasekhar, J.D. Madura,; R.W. Impey, M.L. Klein, Comparison of simple potential functions for simulating liquid water, J. Chem. Phys. 79 (1983) 926–935.

Table, Figure, and Scheme Legends

Table 1. Inhibitory activity of 1,2,3,4-tetrahydrobenzo[*h*][1,6]naphthyridines against AChE and BChE.

Table 2. Permeability values and predicted brain penetration of the novel 1,2,3,4-benzo[*h*][1,6]naphthyridines from the PAMPA-BBB assay.

Fig. 1. Structure of the pyrano[3,2-*c*]quinoline derivative **1** and the peripheral site AChE inhibitor propidium iodide.

Fig. 2. Lineweaver-Burk plots illustrating mixed-type inhibition of AChE-mediated acetylthiocholine hydrolysis by compound (A) **14a** and (B) **16a**. ATCh = acetylthiocholine; v = initial velocity rate.

Fig. 3. (A) Back-titration of the propidium–AChE complex by compounds **16a**, **17a**, and **18a** (2.0 μM EeAChE, 8.0 μM propidium, Tris HCl 1.0 mM , pH 8.0); (B) Determination of K_D value for most active derivative **16a**. K_D value is calculated from the antilog of the Y-intercept value [22b]. P stands for propidium iodide and I stands for tested inhibitor; Fe is the initial fluorescence intensity when enzyme sites are saturated with P, F_P is the fluorescence intensity when propidium is completely displaced from the enzyme, and F denotes the fluorescence intensity after adding a determined amount of displacing agent during the titration experiment.

Fig. 4. (A) Representation of the binding mode of compound **16a** (in orange) obtained at the end of the 100 ns MD trajectory. The side chains or backbone units of the residues involved in interactions are shown as green-colored sticks. Water molecules that mediate interactions of the ligand are shown as red spheres. Propidium is shown as grey sticks. (B) Superposition of the compounds **16a** (orange) and **18a** (cyan) as found at the end of the MD trajectories.

Scheme 1. Synthesis of the target 1,2,3,4-tetrahydrobenzo[*h*][1,6]naphthyridines.

Table 1

Inhibitory activity of 1,2,3,4-tetrahydrobenzo[*h*][1,6]naphthyridines against AChE and BChE.[a]

Compound	*Ee*AChE IC_{50} (μM)	hAChE IC_{50} (μM)	hBChE IC_{50} (μM) or % inhibition at 30 μM
	1st generation		
9a	5.21 ± 0.33	4.15 ± 0.16	8.41%
9b	> 30[b]	13.0 ± 0.8	4.42%
9c	13.6 ± 1.8	> 25[c]	5.54%
10a	6.33 ± 0.96	> 25[d]	8.68%
10b	1.97 ± 0.17	1.06 ± 0.09	nd[e]
10c	6.62 ± 0.62	> 25[f]	6.61%
12a	0.281 ± 0.031	> 25[g]	20.3%
13a	> 30[h]	> 25[i]	12.4%
14a	5.48 ± 0.51	0.801 ± 0.069	25.3%
17a	0.147 ± 0.014	0.942 ± 0.038	nd[e]
	2nd generation		
12b	0.148 ± 0.017	22.8 ± 1.6	27.5%
16a	0.046 ± 0.006	0.065 ± 0.003	0.92 ± 0.03
18a	0.532 ± 0.030	0.556 ± 0.024	1.37 ± 0.07
18b	2.15 ± 0.20	15.8 ± 0.9	2.59 ± 0.14
Tacrine	nd[e]	0.424 ± 0.021[j]	0.046 ± 0.003[j]
Propidium	nd[e]	32.3 ± 2.2[j]	13.2 ± 0.4[j]

[a] IC_{50} inhibitory concentration (μM) of *Electrophorus electricus* or human recombinant AChE and IC_{50} inhibitory concentration (μM) or % inhibition at 30 μM of human serum BChE. IC_{50} values are expressed as mean ± standard error of the mean (SEM) of at least four experiments (n=4), each performed in duplicate.

[b] 43.7% Inhibition of *Ee*AChE activity at 30 μM.

[c] 13.8% Inhibition of hAChE at 25 μM.

[d] 10.0% Inhibition of hAChE at 25 μM.

[e] Not determined.

[f] 15.7% Inhibition of hAChE at 25 μM.

[g] 17.8% Inhibition of hAChE at 25 μM.

[h] 33.7% Inhibition of *Ee*AChE activity at 30 μM.

[i] 10.2% Inhibition of hAChE at 25 μM.

[j] Data taken from ref [18], involving the same experimental conditions.

Table 2

Permeability values and predicted brain penetration of the novel 1,2,3,4-benzo[*h*][1,6]naphthyridines from the PAMPA-BBB assay.

Compound	P_e (10^{-6} cm s^{-1})[a]	Prediction
9a	13.3 ± 3.75	CNS+
9b	12.2 ± 1.54	CNS+
9c	16.8 ± 1.29	CNS+
10a	8.10 ± 1.13	CNS+
10c	9.50 ± 1.05	CNS+
12a	9.70 ± 1.03	CNS+
12b	14.6 ± 1.15	CNS+
13a	26.0 ± 3.87	CNS+
14a	7.70 ± 0.94	CNS+
16a	22.9 ± 0.78	CNS+
18a	5.60 ± 0.58	CNS+
18b	2.40 ± 0.73	CNS+/–

[a] Values are expressed as the mean ± SD of three independent experiments.

Figure 1

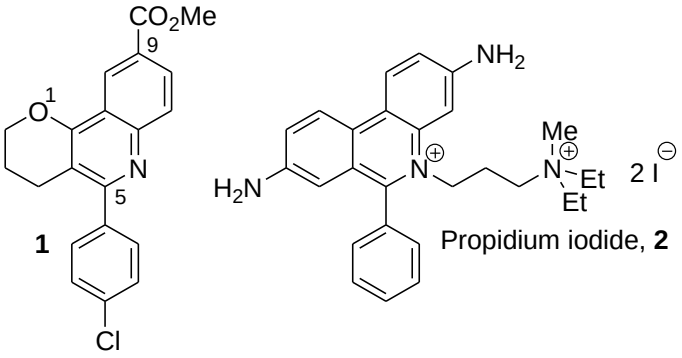

1

Propidium iodide, **2**

Figure 2A

Click here to download high resolution image

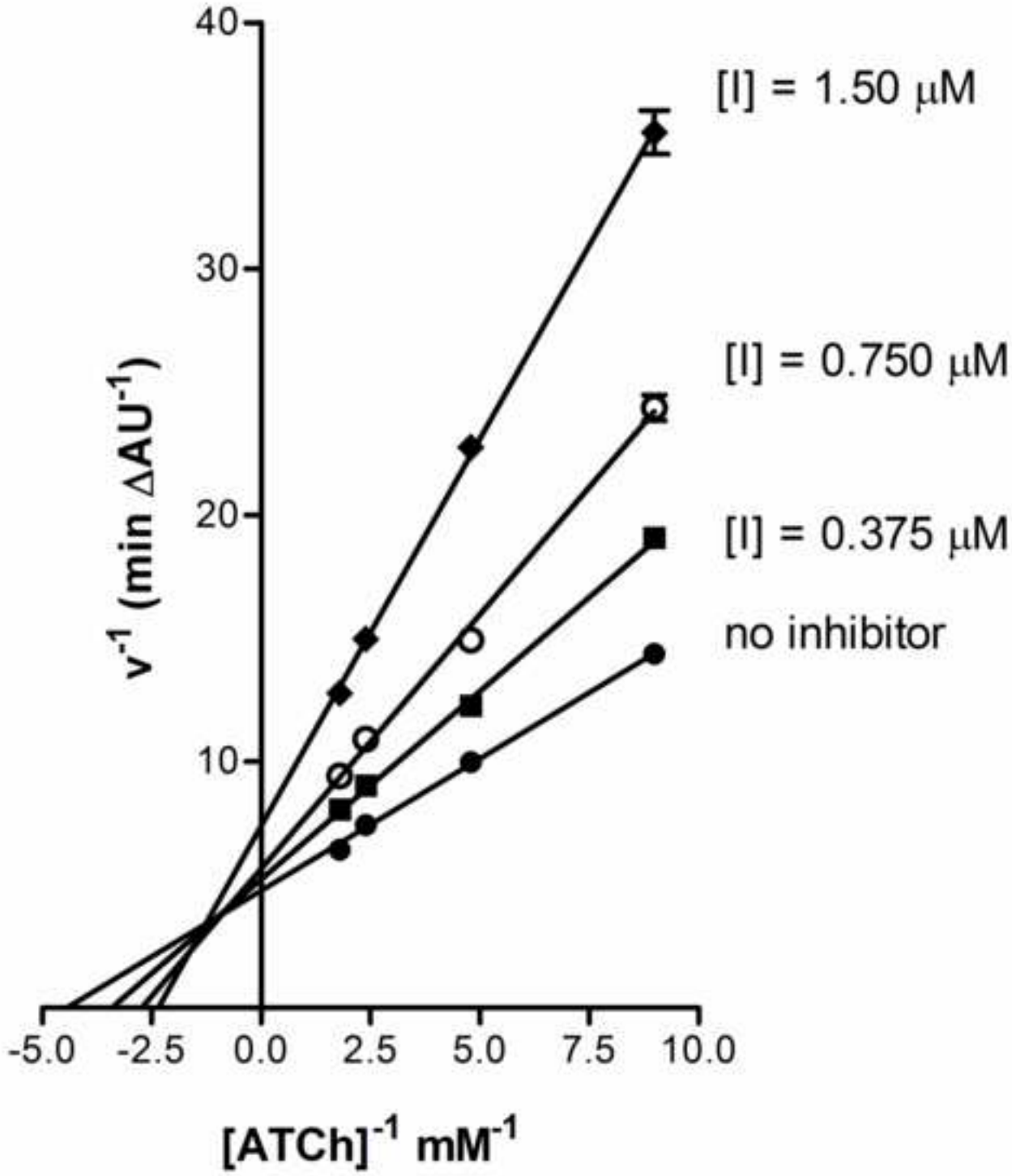

Figure 2B
Click here to download high resolution image

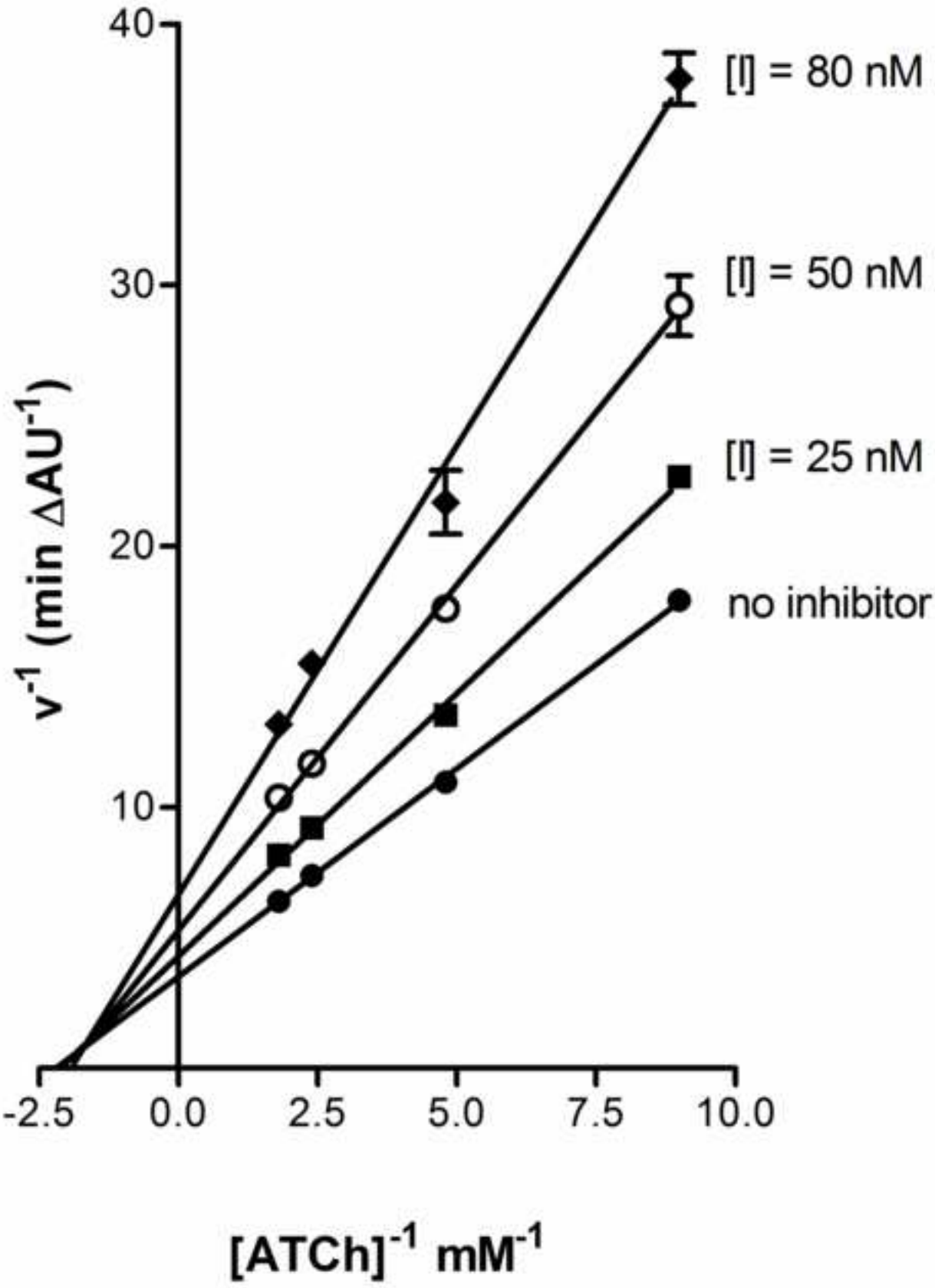

Figure 3A

Click here to download high resolution image

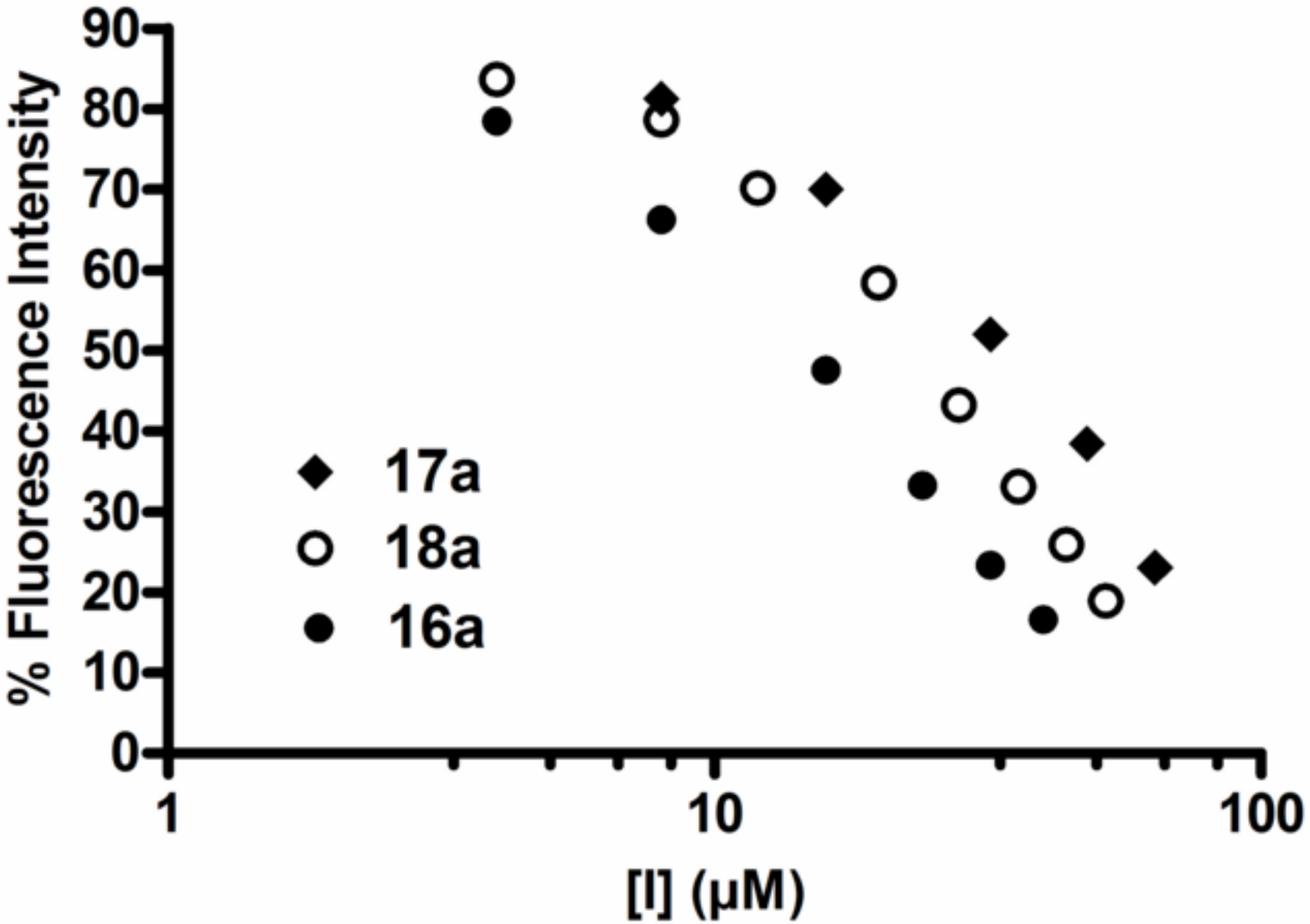

Figure 3B

Click here to download high resolution image

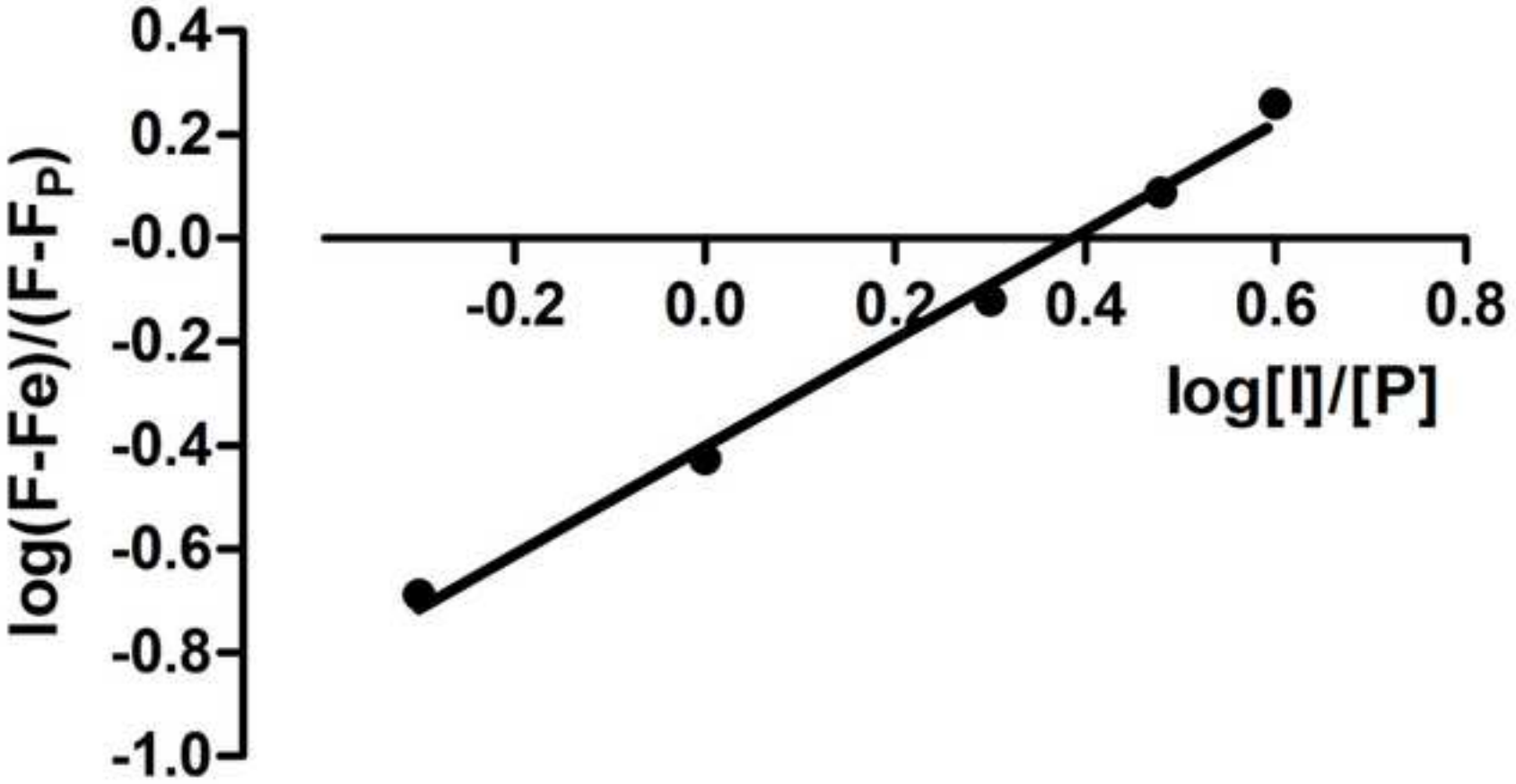

Figure 4A

Click here to download high resolution image

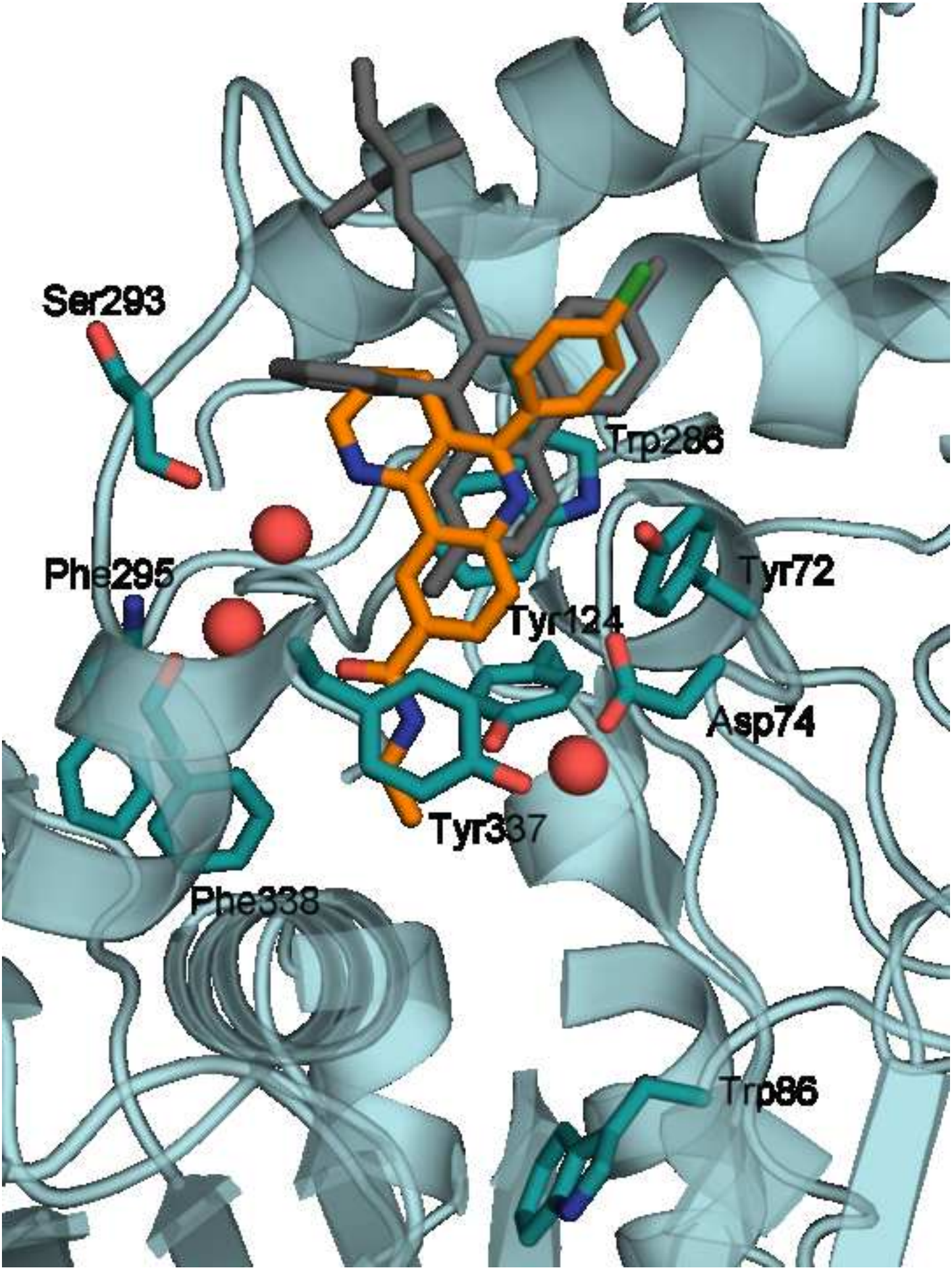

Figure 4B

Click here to download high resolution image

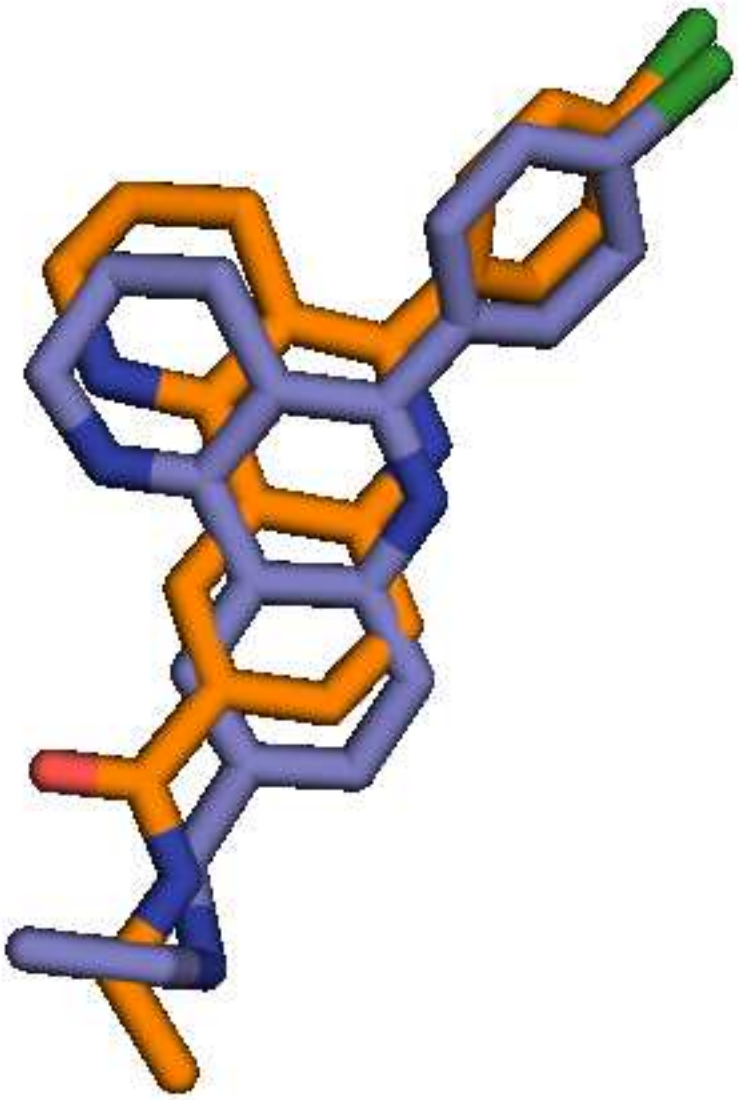

Scheme 1

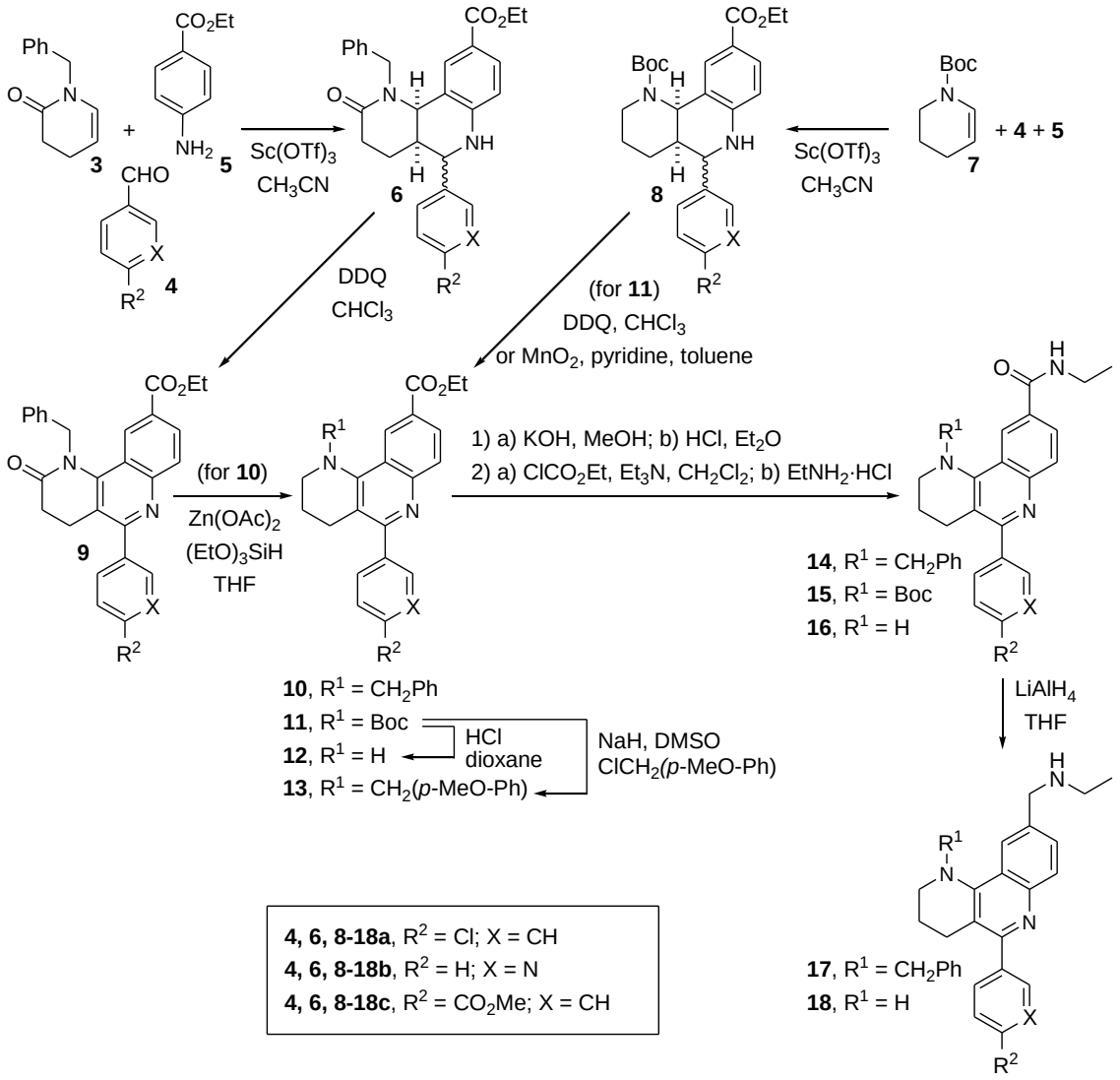
Ph
O
N
3
+
CO2Et
NH2
5
CHO
X
R2
4
Sc(OTf)3
CH3CN
CO2Et
Ph
O
N
H
NH
H
6
X
R2
DDQ
CHCl3
Boc
N
H
NH
H
8
X
R2
(for 11)
DDQ, CHCl3
or MnO2, pyridine, toluene
Sc(OTf)3
CH3CN
Boc
N
7
+ 4 + 5
CO2Et
Ph
O
N
N
9
X
R2
(for 10)
Zn(OAc)2
(EtO)3SiH
THF
CO2Et
R1
N
N
X
R2
10, R1 = CH2Ph
11, R1 = Boc
12, R1 = H
13, R1 = CH2(p-MeO-Ph)
HCl
dioxane
NaH, DMSO
ClCH2(p-MeO-Ph)
1) a) KOH, MeOH; b) HCl, Et2O
2) a) ClCO2Et, Et3N, CH2Cl2; b) EtNH2·HCl
H
N
O
R1
N
N
X
R2
14, R1 = CH2Ph
15, R1 = Boc
16, R1 = H
LiAlH4
THF
17, R1 = CH2Ph
18, R1 = H
4, 6, 8-18a, R2 = Cl; X = CH
4, 6, 8-18b, R2 = H; X = N
4, 6, 8-18c, R2 = CO2Me; X = CH

Supplementary Material - For Publication Online

Click here to download Supplementary Material - For Publication Online: Revised_SupplementaryMaterial_MunozTorrero_Lavilla